DOKUZ EYLÜL UNIVERSITY
GRADUATE SCHOOL OF NATURAL AND APPLIED SCIENCES

THE EFFECT OF LOCAL SITE CHARACTERISTICS ON THE RESULTS OF ONE-DIMENSIONAL DYNAMIC SITE RESPONSE ANALYSIS

by

Serdar TİMUR

March, 2023

İZMİR

THE EFFECT OF LOCAL SITE CHARACTERISTICS ON THE RESULTS OF ONE-DIMENSIONAL DYNAMIC SITE RESPONSE ANALYSIS

A Thesis Submitted to the

Graduate School of Natural and Applied Sciences of Dokuz Eylül University

In Partial Fulfillment of the Requirements for Master of Degree in Civil Engineering, Geotechnical Engineering Program

by

Serdar TİMUR

March, 2023

İZMİR

MASTER OF SCIENCE THESIS EXAMINATION RESULT FORM

We have read the thesis entitled **"THE EFFECT OF LOCAL SITE CHARACTERISTICS ON THE RESULTS OF ONE-DIMENSIONAL DYNAMIC SITE RESPONSE ANALYSIS"** completed by **SERDAR TİMUR** under supervision of **ASST. PROF. DR. MEHMET KURUOĞLU** and we certify that in our opinion it is fully adequate, in scope and in quality, as a thesis for the degree of Master of Science.

Asst. Prof. Dr. Mehmet KURUOĞLU

_____

Supervisor

Prof. Dr. Gürkan ÖZDEN

_____

(Jury Member)

Asst. Prof. Dr. Tuğba ESKİŞAR

_____

(Jury Member)

_____

Prof. Dr. Okan FISTIKOĞLU

Director

Graduate School of Natural and Applied Sciences

ACKNOWLEDGEMENTS

I would like to thank my advisor, Asst. Prof. Dr. Mehmet Kuruoğlu, for his detailed help and guidance during my thesis work. I would like to thank Prof. Dr. Gürkan ÖZDEN for his notable contributions and helps during my thesis study.

Serdar TİMUR

THE EFFECT OF LOCAL SITE CHARACTERISTICS ON THE RESULTS OF ONE-DIMENSIONAL DYNAMIC SITE RESPONSE ANALYSIS

ABSTRACT

In the scope of this thesis, Bayraklı region has been chosen to investigate the significance of local soil conditions on the 2020 Samos Earthquake and has been performed on dynamic site response. DEEPSOIL software has been used to perform analyses at D, E, R, YG, and Y sites. The deconvolution method has been used to reduce at Çamdibi station (3522) surface records of the 2020 Samos earthquake to stiff soil levels. The amplification effects of these records on different five sites have been examined using rock-level records. Despite the low energy of the 2020 Samos earthquake, the spectral amplifications obtained in the analysis have been expressed by the fact that the damping of the soil has been not activated.

The same soil profile has been analyzed using two different backbone models (MKZ and GQ/H) for R site and results of analyses have been compared. It has been observed that the differences in impedance, which represent the difference in shear wave velocities between layers, and differences in the target shear strength at various depths within the soil profile had a significant impact on the results obtained from each model. This emphasizes the significance of selecting an appropriate backbone model for conducting dynamic soil behavior analysis as different models can yield different results depending on the characteristics of the soil profile being analyzed.

The effect of degradation in soil strength on the variation of predominant period acceleration-time records with different predominant periods has been investigated at for E, R, and YG sites. It has been concluded that soil liquefaction and softening has a significant effect on the frequency content of seismic ground motions.

Keywords: Site response analysis, spectral acceleration, amplification ratio, liquefaction, Izmir

YEREL ZEMİN KOŞULLARININ BİR-BOYUTLU DİNAMİK YER TEPKİ ANALİZ SONUÇLARI ÜZERİNE ETKİSİ

ÖZ

Bu tez kapsamında, yerel zemin koşullarının dinamik zemin davranışı üzerindeki önemini araştırmak için Bayraklı bölgesi seçilmiştir ve dinamik saha tepki analizleri yapılmıştır. DEEPSOIL yazılımı D, E, R, YG ve Y sahalarında analizler yapmak için kullanılmıştır. Ters evirişim yöntemi ile, 2020 Samos depreminin Çamdibi istasyonundaki (3522) yüzey kayıtları rijit zemin seviyelerine indirilmiştir. Ters evirişim yöntemiyle elde edilen kayıtlar kullanılarak, farklı sahalardaki büyütme etkileri incelenmiştir. 2020 Samos depreminin düşük enerjisine rağmen, analizde elde edilen spektral büyütmeler, zeminin sönümünün aktif hale gelmemesi ile açıklanmıştır.

Aynı zemin profili iki farklı omurga modeli (MKZ ve GQ/H) kullanılarak analiz edilmiş ve analiz sonuçları karşılaştırılmıştır. Analizler, tabakalar arasındaki kayma dalgası hızlarındaki farkı temsil eden empedanstaki farklılıkların ve zemin profili içindeki çeşitli derinliklerdeki hedef kayma dayanımı farklılıklarının, her bir modelden elde edilen sonuçlar üzerinde önemli bir etkiye sahip olduğunu göstermiştir. Farklı modeller incelenmekte olan zemin profilinin özelliklerine bağlı olarak değişen sonuçlar üretebileceğinden, bu durum zemin davranışı analizleri yapmak için uygun bir model seçmenin önemini vurgulamaktadır.

Zemin mukavemetindeki azalımın farklı baskın periyotlarla sahip ivme zaman kayıtlarının baskın periyotlarının değişimi üzerindeki etkisi E, R ve YG sahalarında araştırılmıştır. Zemin sıvılaşması ve yumuşamasının sismik yer hareketlerinin frekans içeriği üzerinde önemli bir etkiye sahip olduğu sonucuna varılmıştır.

Anahtar Kelimeler: Yer tepki analizleri, spektral ivme, büyütme oranı, sıvılaşma, İzmir.

CONTENTS

Page

M.SC THESIS EXAMINATION RESULT FROM…….....ii

ACKNOWLEDGEMENTS…… iii

ABSTRACT.....iv

ÖZ.....v

LIST OF FIGURES x

LIST OF TABLES.....xv

CHAPTER 1-INTRODUCTION.....1

1.1 Case Stories……2

1.1.1 1967 Caracas Earthquake……...2

1.1.2 1985 Mexico City Earthquake……...3

1.1.3 1989 Loma Prieta Earthquake……6

CHAPTER 2-THEORETICAL BACKGROUND SITE RESPONSE ANALYSIS.....11

2.1 Site Classification Methodology……..11

2.2 One-Dimensional (1D) Site Response Analysis (SRA) Methods……15

2.2.1 Equivalent Linear (EL) Analysis……...……...16

2.2.1 Nonlinear Analysis Method……17

2.3 Dynamic Soil Properties……...18

2.4 Backbone Models…… 23

2.4.1 Modified Kondner & Zelesko (MKZ) Model……...……23

2.4.2 Generalized Quadratic Hyperbolic (GQ/H) Model…….27

2.5 Excess Pore Water Pressure (PWP) Models…….30

2.5.1 Matasovic & Vucetic model for clay soils……...…….31

2.5.2 Dobry & Vucetic model for sand soils……..33

CHAPTER 3-ANALYSIS METHOD AND PROPERTIES OF SITE CHARACTERISTICS……...……...…….37

3.1 Analysis Method…….....37

3.2 Properties of site characteristics……...……38

CHAPTER 4 – CASE STUDIES……..45

4.1 Case-1 (Determination 2020 Samos Earthquake on Bayraklı Soil) ……...45

4.1.1 Deconvolution Procedure…….....…….45

4.1.2 Result of Analysis …….……49

4.2 Case-2 (Comparison of MKZ and GQ/H Model) ……...…….……54

4.2.1 Result of Analysis……...……...……...55

4.3 Case-3 (Liquefaction and softening of soil on design spectra)..…….…. 57

4.3.1 Input Motion Selection……...…….....58

4.3.2 Result of Analysis…….……....59

CHAPTER 5 – CONCLUSIONS AND RECOMMENDATIONS…….....66

REFERENCES…….....69

LIST OF FIGURES

Page

Figure 1.1 Variation potential damage index with structural period and soil depth……3
Figure 1.2 Subsoil profile basin of valley Mexico City…….....4
Figure 1.3 Changing of shear modulus decrement with cyclic shear strain amplitude...4
Figure 1.4 Variation of damping with cyclic shear strain amplitude…..……....5
Figure 1.5 Variation building damage intensity with number of stories…….……5
Figure 1.6 Variation of spectral acceleration at different sites……...…6
Figure 1.7 Time histories of acceleration recorded on different soil conditions……6
Figure 1.8 Acceleration time history record at UNAM and SCT sites…….....8
Figure 1.9 Variation of peak horizontal acceleration at Rock and Soil sites with distance during 1989 Loma Prieta earthquake …….……8
Figure 1.10 Acceleration time history records at Santa Cruz and at Rincon Hill in San Francisco.….....9
Figure 1.11 Average normalized spectral acceleration for rock motions recorded …....9
Figure 1.12 Variation of acceleration in soft soil and rock sites with increasing intensity …….…….. 10
Figure 2.1 Spectral acceleration for different local soil conditions……..……13
Figure 2.2 Short period amplification coefficient……...13
Figure 2.3 Long period amplification coefficient ……...14
Figure 2.4 Comparison previous and new site classification code regulations……. .14
Figure 2.5 Propagation of seismic motions from bedrock to surface…….…..15
Figure 2.6 Iterative procedure in equivalent linear analysis method……16
Figure 2.7 Dynamic soil response (stress-strain path) according to extended Masing……...17
Figure 2.8 Influence of mean confining stress on shear modulus decrement relation for clays with variation of plasticity indices……20
Figure 2.9 Influence of plasticity index on shear modulus decrement with increasing strain.....21
Figure 2.10 Influence of plasticity index on damping with increasing strain.....21

Figure 2.11 Effect of plasticity index on spectral acceleration……22
Figure 2.12 Effect of soil deposit thickness on spectral acceleration……...22
Figure 2.13 Variation of parameters B and s with increasing effective confining pressure……24
Figure 2.14 Comparison of MKZ and KZ model.....25
Figure 2.15 Variation of viscous damping using Rayleigh damping formulation according to period and frequency…….……...26
Figure 2.16 Comparison of the dynamic response of soils of different depths for different soil models in the Meoland site ……...27
Figure 2.17 Comparison of damping ratio obtained masing rules and test result..... 28
Figure 2.18 Comparison the relationship (a) shear modulus reduction curves and (b) damping according to different fitting models ……...…29
Figure 2.19 The methodology for occurring the Generalized Non-Masing Hysteresis Model …….……...….29
Figure 2.20 Comparison of Darendeli (2001) reference curve, generalized non-masing and masing hysteresis model……...30
Figure 2.21 Variation of t parameter depending on plasticity index…..……...32
Figure 2.22 Effect of over-consolidation ratio and number of cycles on degradation index……...33
Figure 2.23 Comparison of laboratory determined and calculated PWP mechanism: (a) v=1, (b) v=3.8……..35
Figure 2.24 (a) Influence of Dr on PWP mechanism (Dobry, 1982); and (b) effect of Cu on PWP mechanism (Li, 2013) …….36
Figure 2.25 (a) Suggested relationship to predict F factor; and (b) comparison of relation reproduced from stress-based experiments with data from strain-based experiments from Kenan (2005) ……..…36
Figure 3.1 Variation of shear wave velocity with depth for five different sites……....39
Figure 4.1 Idealized soil profile 3522 station…….….....47
Figure 4.2 Shear modulus reduction of clay soils used in deconvolution method……48
Figure 4.3 Variation of damping ratio of clay soils used in deconvolution method…48
Figure 4.4 Shear modulus reduction curve of cohesionless soils used in deconvolution method……...49

Figure 4.5 Variation damping ratio of cohesionless soils used in the deconvolution method……..49
Figure 4.6 E component of the acceleration record at the surface and outcrop…....52
Figure 4.7 N component of acceleration record at the surface and outcrop……..….52
Figure 4.8 Spectral acceleration period for different local soil sites according to component outcrop E……...52
Figure 4.9 Amplification factor (AF) for different local soil sites according to component outcrop E……..…53
Figure 4.10 Spectral acceleration period for different local soil sites according to component outcrop N…….53
Figure 4.11 Amplification factor (AF) for different local soil sites according to component outcrop N……....54
Figure 4.12 Variation of shear wave velocity with depth for R site……..55
Figure 4.13 Comparison of implied shear strength for R sites according to backbone models…….55
Figure 4.14 Comparison of shear strain for R site according to backbone models…….56
Figure 4.15 Comparison of PGA (g) for R site according to backbone models…… …57
Figure 4.16 Comparison of PWP generation for R site according to backbone models……...57
Figure 4.17 Comparison of spectral acceleration generation for R site according to backbone models…….....58
Figure 4.18 Variation excess pore water pressure generation with depth for E site...60
Figure 4.19 Variation excess pore water pressure generation with depth for YG site..61
Figure 4.20 Variation excess pore water pressure generation with depth for R site….61
Figure 4.21 Variation of predominant period of input motions with depth for E site...62
Figure 4.22 Variation of predominant period of input motions with depth for YG site.....62
Figure 4.23 Variation of predominant period of input motions with depth for R site...63
Figure 4.24 Spectral acceleration period graph for E site…….63
Figure 4.25 Spectral acceleration period graph for YG site…….64

Figure 4.26 Spectral acceleration period graph for R site……64
Figure 4.27 Variation of maximum velocity/maximum acceleration with depth for E site.....64
Figure 4.28 Variation of maximum velocity/maximum acceleration with depth for YG site.....65
Figure 4.29 Variation of maximum velocity/maximum acceleration with depth for R site.....65

LIST OF TABLES

Page

Tablo 3.1 Soil Properties D site……...39

Tablo 3.2 Soil Properties of E site……...……..……...40

Tablo 3.3 Soil properties of R site……41

Tablo 3.4 Soil properties of Y site…….....42

Tablo 3.5 Soil properties of YG Site……43

Tablo 4.1 Equivalent linear deconvolution analysis result for east-west direction…...50

Tablo 4.2 Equivalent linear deconvolution analysis result for north-south direction...51

Tablo 4.3 Properties of input motions…….……59

CHAPTER 1

INTRODUCTION

The solution to free field ground motion is a critical and essential step in geotechnical earthquake and structural engineering to reduce the risk of structural damage and loss of life during seismic events. As earthquake waves move from bedrock to the surface, they interact with the ground environment they pass through. This interaction can affect both the soil and any structures embedded in it. Site-specific dynamic analysis aims to understand how changes in the dynamic response of the soil can impact the dynamic oscillation of structures.

Site response analysis provides a means of computing various output parameters, such as spectral acceleration, displacement, shear strain, shear stress, Fourier spectrum, amplification factor, excess pore water pressure, peak ground acceleration, and design response spectra. These parameters are affected by several factors, including the bedrock geometry of the subsoil, the characteristics of the seismic source, the variation in soil types, the dynamic soil properties, lateral discontinuities, and surface topographic features. The most important parameters for response spectra are classified into two groups: vertical and horizontal response spectra. Vertical response spectra are used for the seismic design of nuclear power plants and dams, while horizontal spectra are mainly used for most structures.

The influence of local soil properties on seismic motion and the intensity of devastation is significantly studied using the results of site response analyses and case histories from past earthquakes, such as the 1967 Caracas, 1985 Mexico City, and 1989 Loma Prieta earthquakes. The dynamic motions at the bedrock level may dramatically change in terms of frequency content, amplitude, and duration when the motions are transferred through a soil deposit. The main characteristics and properties of ground motion variations are generally termed as site effects (Seed and Idriss, 1969). Numerically, many computer software programs, such as FLAC, PLAXIS, and DEEPSOIL, conduct these analyses. They differ in geometric dimensions (1D or

2D/3D), solution methods (frequency or time domain), and allow for different numerical schemes and constitutive relationships for cyclic nonlinear and dissipative soil behaviour. Current developments in the field of geotechnical engineering and field-testing methods have permitted researchers to execute elaborate studies on site effects, properly conduct risk assessments, provide detailed information on local soil properties, and perform site response analyses of regions of interest.

Numerically, this is solved as the probation of waves in a continuous medium. However, the wave propagation solution is difficult to predict and includes significant uncertainties. These methods of solution demonstrate the specifications of an effective.

1.1 Case Histories

1.1.1 1967 Caracas Earthquake

On June 29, 1967, the Caracas earthquake occurred with a moment magnitude of 6.3, and its epicenter was 35 km east of the city of Caracas. In the Caracas earthquake, the rock and surface acceleration values are 0.03g and 0.06g, respectively. Despite the low acceleration values at the surface, analyses and field observations were conducted to explain the reasons for the crucial damage led by the dynamic oscillation. In general, the soil of the city consists of sand and gravel with a clay binder, becoming increasingly dense with depth. While the dynamic properties and ordering of soils in the city of Caracas are approximately the same in all parts of the city, the only variable is that the soil depth is variable. Seed used the concept of potential damage index, which defines the relationship between the force that a building must withstand and the earthquake force that occurs in the building. The structures were divided into three groups according to the depth of the ground on which structures were located and their periods. Based on measured values of building periods in Caracas City, these period ranges represent average values for buildings with number of story number 5 to 9, 10 to 14, and 15 to 19, respectively. The potential damage index of structures is calculated for these groups. Figure 1.1 shows the potential damage index of structures according to soil depth and structure period. Figure 1.1 shows that in areas where the soil depth

is less than 100 m, the degree of damage to buildings is at the same level, while in the areas where the soil depth is more than 150 m, the most damaged buildings are the buildings with a floor number greater than fourteen. In addition, Figure 1.1 draws attention to the effect of local soil conditions on dynamic soil-structure interaction.

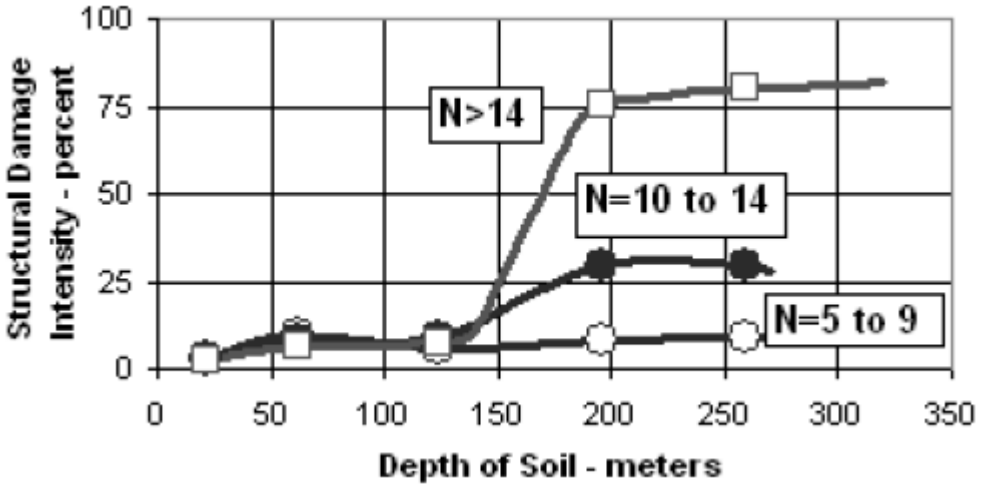


Figure 1.1 Variation damage potential index with structural period and soil depth (Seed, 1974)

1.1.2 1985 Mexico City Earthquake

On September 19, 1985, an earthquake called Mexico City, with a depth of 18 km and a rupture zone of 45 km, took place on the part of the San Andreas fault. The earthquake's hypocenter is depth of 18 km, and its moment magnitude (Mw) is 7. While the south-southwest direction, dominated by the dominant components of the ground motion, did not suffer much damage due to the filtering and reflection caused by the extension directions of the mountains surrounding the city, the east-west region of the city suffered the most damage. Mexico City subsoil conditions located south of the Mexican plateau can be classified as rock zone, transition zone, and old lake bed, as shown in Figure 1.2. The new lakebed underlain on the old lake bed has static and dynamic soil properties such as exhibiting linear stress-strain during dynamic loading behavior due to its high plasticity, low stiffness, water-saturated, very compressible,

and very soft, as illustrated in Figures 1.3, 1.4. Figure 1.5 shows buildings with the highest damage intensity are those 6 to 20 stories high. Also, Figure 1.5 shows that buildings with the predominant period of approximately 2 s suffer the most damage. Figure 1.6 demonstrates that the spectral accelerations on the surface and in the rock obtained under different, since dynamic response of soil are very different. Figure 1.7 indicates that site effects significantly change the frequency content and amplitude of seismic waves. The effective periods of the buildings are extended from 0.1N to 0.2N due to the variation of soil stiffness, cracking of east walls, and inelastic behavior of buildings.

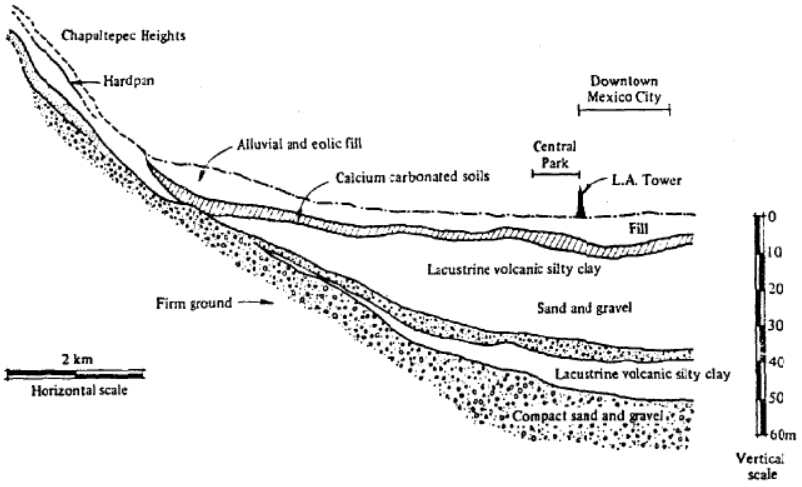


Figure 1.2 Variation of subsoil basin of valley of MEXICO (after Zeevaert, 1972) (Seed et. al., 1987)

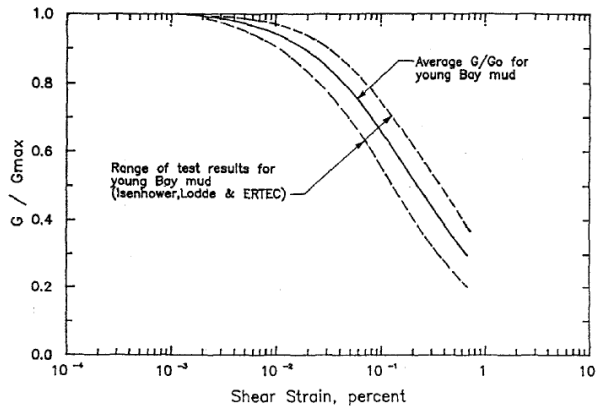


Figure 1.3 Changing of shear modulus decrement with cyclic shear strain amplitude (Seed et al., 1987)

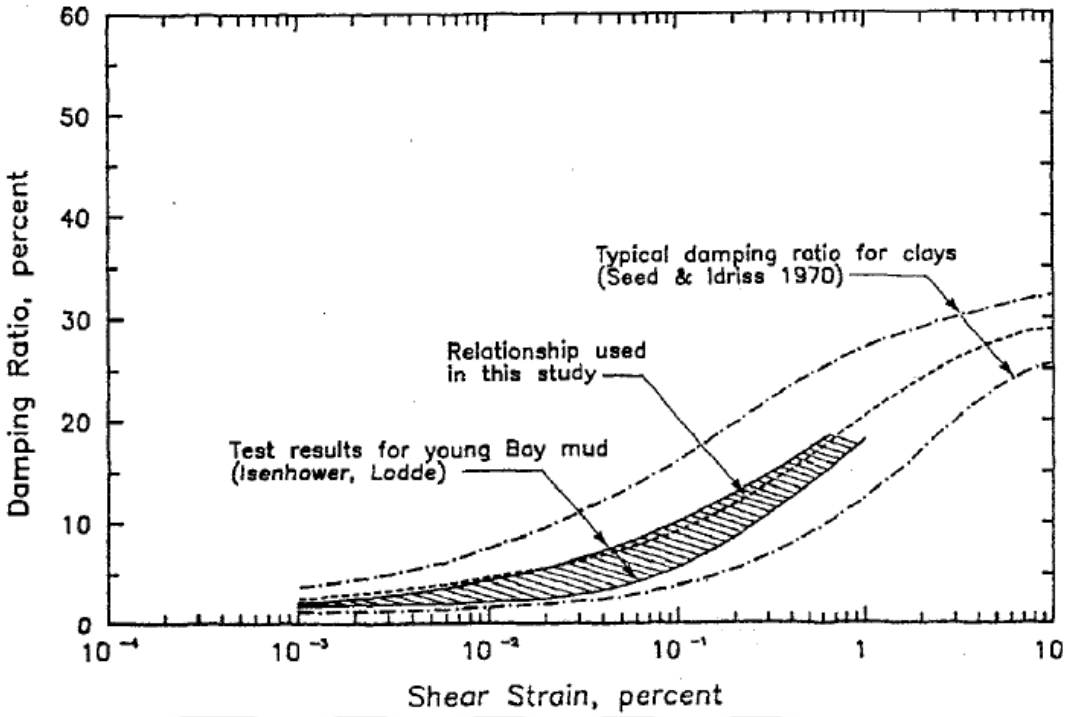


Figure 1.4 Variation of damping with shear strain (Seed et. al., 1987)

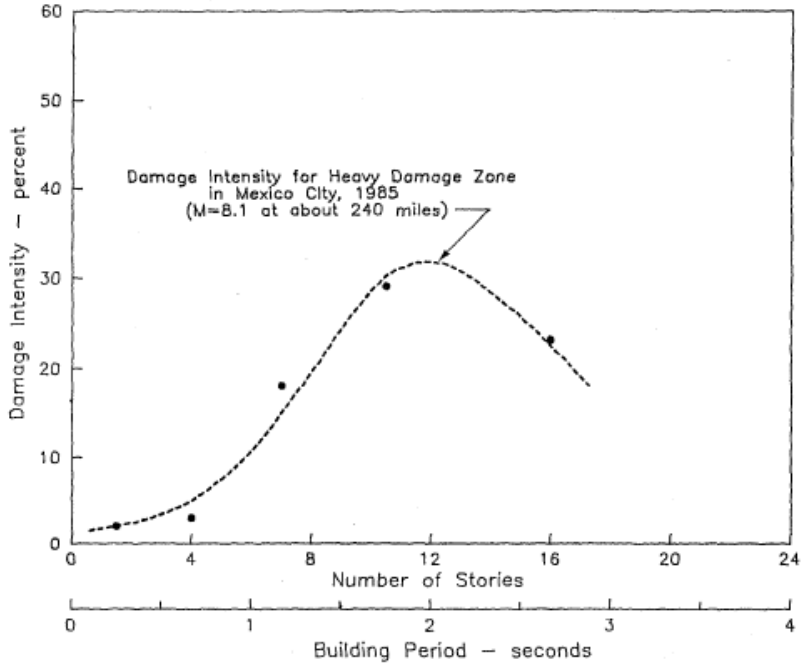


Figure 1.5 Variation building damage intensity with number of stories (Seed et. al., 1987)

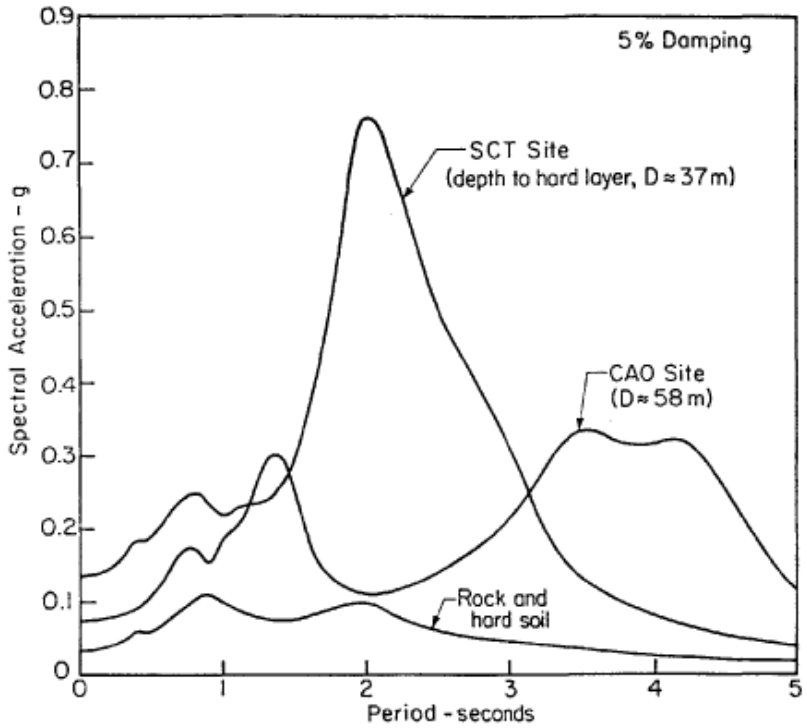


Figure 1.6 Variation of spectral acceleration at different sites (Seed et. al., 1987)

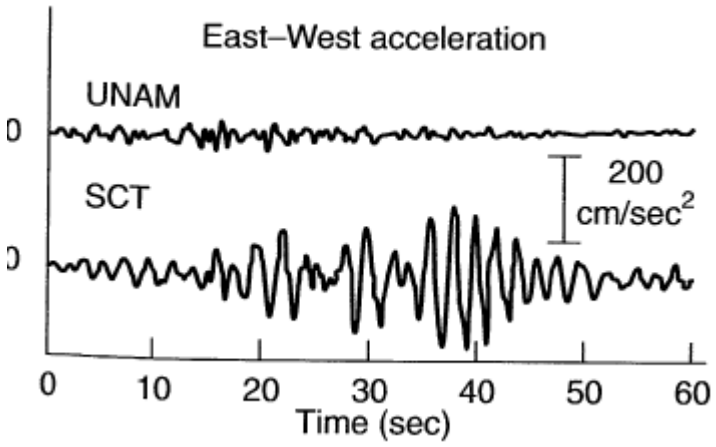


Figure 1.7 Acceleration time history records at UNAM and SCT sites (Kramer, 1996)

1.1.3 1989 Loma Prieta Earthquake

On January 17, 1989, an earthquake called Loma Prieta took place on the part of San Andreas fault, with the depth of 18 km and a rupture zone of 45 km. The earthquake's hypocenter is a depth of 18 km, and its moment magnitude (Mw) is 7. The Loma Prieta Earthquake has drawn attention to topics in geotechnical earthquake engineering. While the first issue is liquefaction occurring in areas such as San Francisco, the second issue is the effect of site effect on ground motion. Figure 1.8 demonstrates maximum horizontal acceleration values at 70 soils and 33 rock sites, while Figure 1.9 demonstrates peak horizontal acceleration values at 9 soft soil sites. Peak horizontal values recorded in 9 soft soil, 70 soils, and 33 rocks are shown in Figure 1.8. Figure 1.8 shows that the records obtained in rock and typical soil areas agree with the results obtained from empirical relations. In contrast, Figure 1.9 shows that the records obtained in the soft soil areas and the results obtained from the empirical relations do not agree. Figure 1.9 shows that the variation of horizontal acceleration on soft soils varies between about 0.1 g and 0.3 g at distances of 45-100 km from the source. In contrast, the Figure 1.8 shows that the horizontal acceleration between two identical hard soils varies between 0.05 g and 0.18 g. The local soil effect significantly changes frequency content and amplitude of the Loma Prieta Earthquake. As illustrated in Figure 1.10, while the predominant period of earthquake wave is 0.32 s in Rincon Hill in San Francisco, which is 20 km away from the source, the predominant period of earthquake wave is 0.48 s in Santa Cruz, which is 80 km away from the source. The spectral acceleration in region Santa Cruz is more significant than in region Rincon Hill because region Santa Cruz is closer to the source than region Rincon Hill, as shown in Figure 1.11. In addition, it is shown in the Rincon Hill region that spectral acceleration in the Santa Cruz region is more effective in the crest region in broader and more extended long periods, as illustrated in Figure 1.11. In the Mexico City and Loma Prieta Earthquakes, as the energy of input the motion increases, it is seen that the input motion tends to deamplified in soft soils. At the same time, it tends to increase the input motion in weak ground motions, as shown in Figure 1.12.

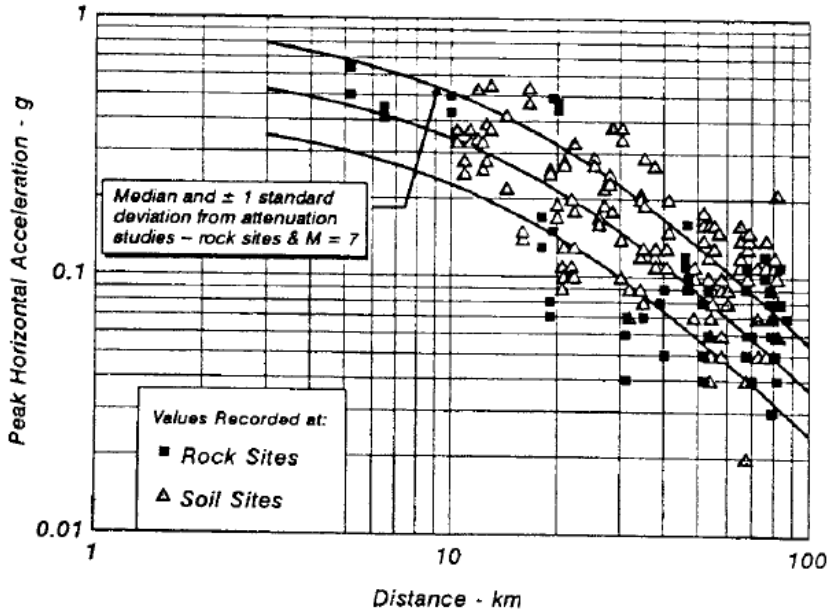


Figure 1.8 Variation of maximum horizontal acceleration with way for Rock and soil sites (Idriss, 1990)

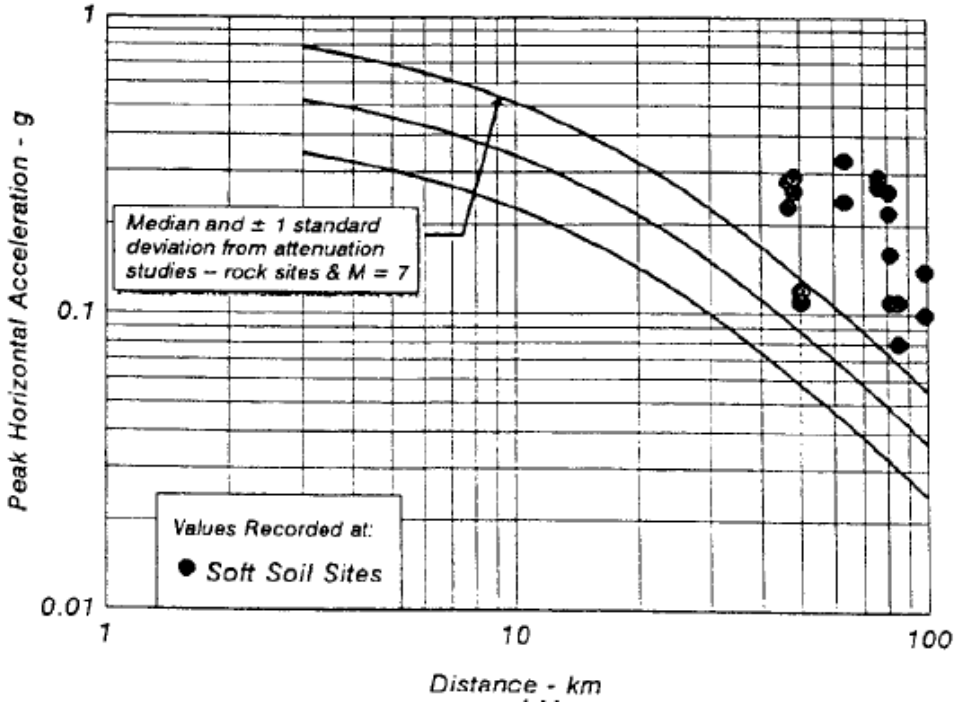


Figure 1.9 Variation peak horizontal acceleration with distance for soft soil sites (Idriss, 1990)

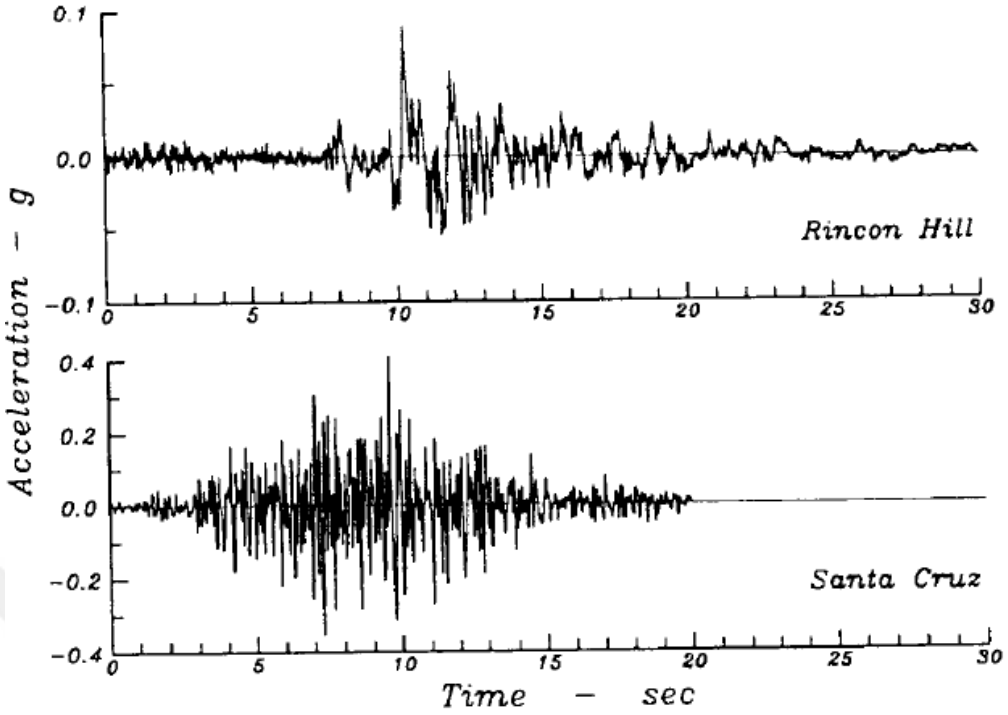


Figure 1.10 Acceleration-time record at Santa Cruz and rincon Hill region (Idriss, 1990)

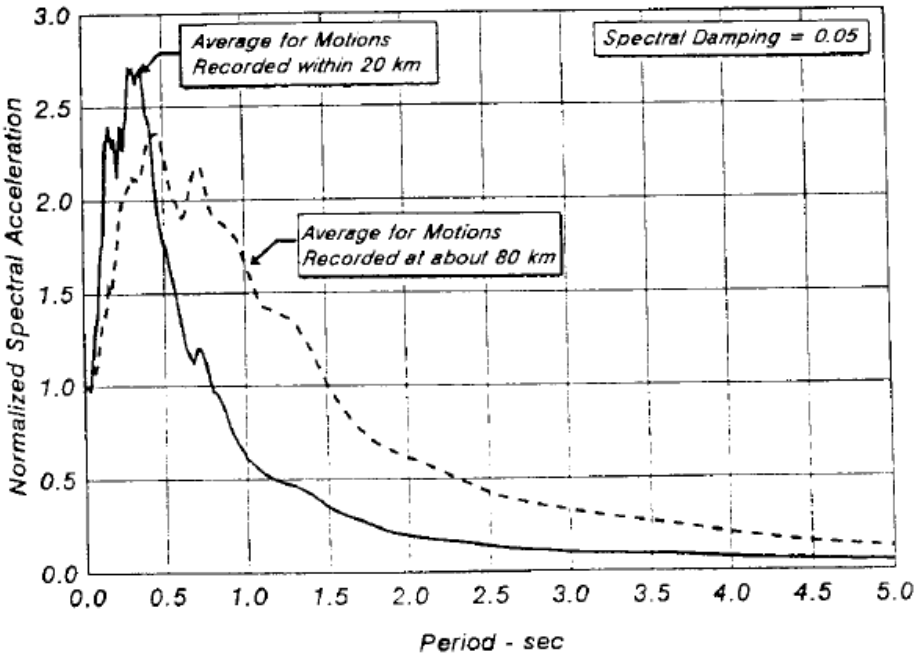


Figure 1.11 Spectral Accelerations at Santa Cruz and Rincon Hill regions (Idriss, 1990)

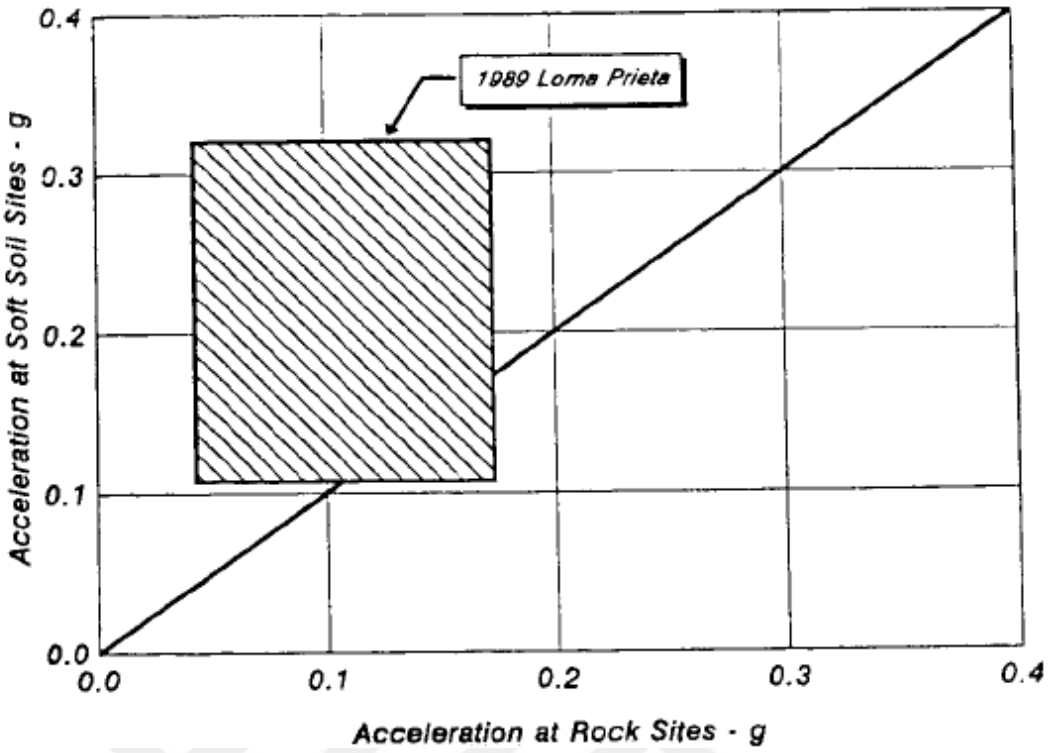


Figure 1.12 Variation of acceleration in soft soil and rock sites with increasing intensity (Idriss, 1990)

CHAPTER 2

THEORETICAL BACKGROUND OF SITE RESPONSE ANALYSIS

2.1 Soil Classification Methodology

Seismic code regulations are needed to design structures reliably and economically, to protect these structures against a possible seismic hazard, or to reduce the damage caused by the seismic hazard. Researchers have continually revised seismic code regulations introduced in 1942, increasing knowledge and application methods in geotechnical and structural engineering. The seismic code regulations capture the impact of dynamic response of soil on ground motion with these progressing developments.

The Uniform Building Code (UBC) edition in 1985 was introduced the soil deposit factor: S1, S2, and S3 correspond to rock, deep soil, and soft soil profiles. After, it was introduced that soft soils significantly change soil type (S4), representing deep soft soils as illustrated in the Figure 2.1. UBC does not evaluate soil amplifications as it is a strength-based regulation.

The new site classification method proposed by the Borcherd (1994) is based on data from regions and empirical correlations obtained after correlating these data using shear wave velocity and analyzing these data using strong Loma Prieta earthquake records. Borcherd (1994) summarizes in four steps the generation of a five percent damped spectral based on shear wave velocity and the effect of input ground motion. The first step has been determined the input motion. In the second step, the sites are classified using shear wave velocity. The next step adjusts the amplification factors for short and long period using two steps, as shown in Figures 2.2 and 2.3. In the last step, the shape of the design response spectra with five percent damped is obtained using the amplification coefficients obtained in the third step. Previous seismic code regulations divide into four S1-S4, while the new site classification divides it into classes, from A to F, as shown Figure 2.4. The site classification method, including

local soil classes and amplification parameters in the short and long period regions, adjusts to recent earthquake building code regulations to show the impact of local soil properties on the design spectral acceleration. Undrained shear strength, shear wave velocity, and standard penetration resistance number in the upper 30 meters are used for determination site class type. Site-specific dynamic soil behavior analyses are required for sites with liquefaction risks, such as ZD and ZF soil class types.

Horizontal elastic design spectra are created according to spectral acceleration and local soil effect coefficients in Turkey Earthquake Hazard Map at the website (https:/tdth.afad.gov.tr), excluding the ZF soil class. The map acceleration Ss and S1 are transformed to design spectra parameters Sds and Sd1 by multiplying them with local soil amplification parameters. Ss and S1 correspond to design spectral acceleration factors for the short and long-period regions. Fs and F1 correspond to local soil conditions parameters short and long period regions.

Site specific dynamic soil behavior analyses are required for sites with liquefaction risks, such as the ZF and ZD soil class types. Site classification can also be made based on undrained shear strength and expected standard penetration test results when shear wave velocity is unavailable. There are drawbacks of standard penetration experiment and undrained shear strength. Standard penetration experiment may give false results due to boiling sand layers, and undrained shear strength is for water-saturated clays and elastic silts.

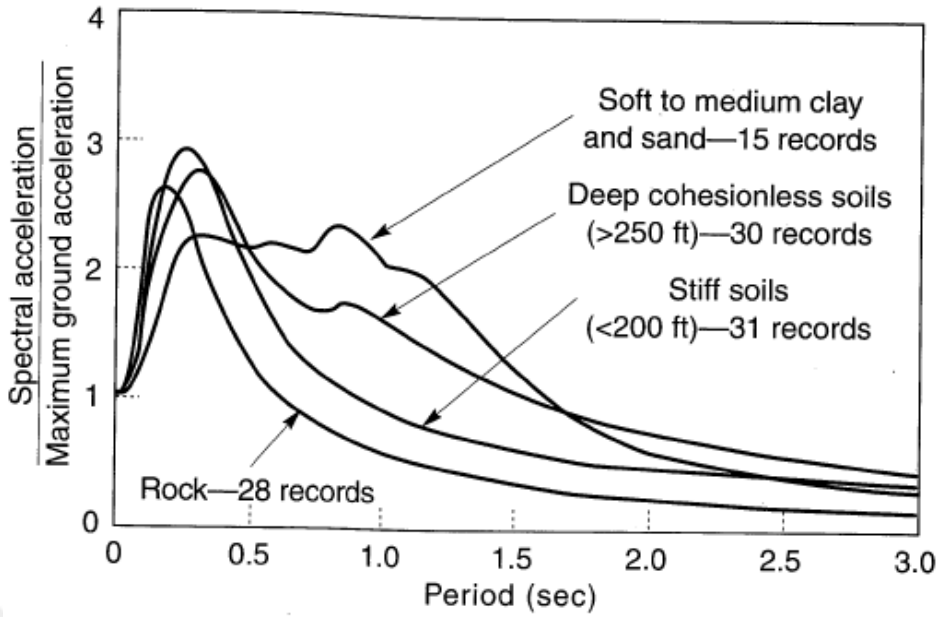


Figure 2.1 Spectral acceleration for different local soil conditions (Seed et al. 1976a, b)

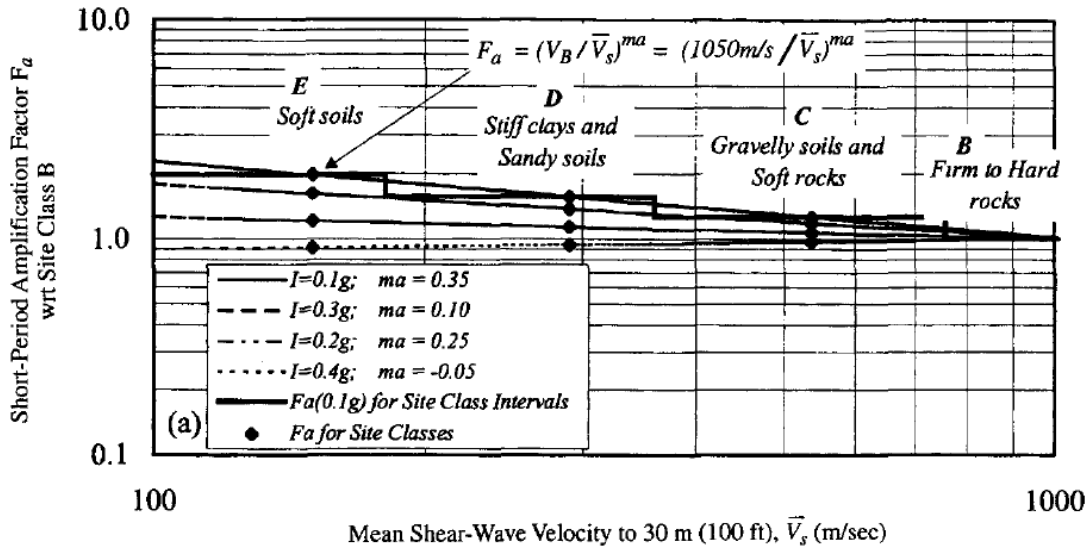


Figure 2.2 Variation of amplification coefficient for short-period region with shear wave velocity (Borchert, 1994)

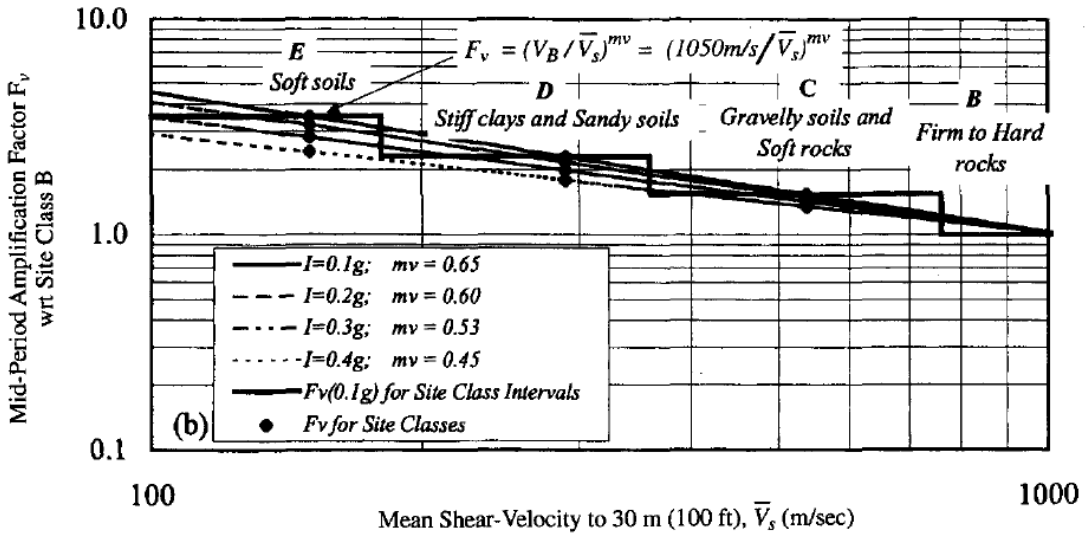


Figure 2.3 Variation of amplification coefficient for short-period region with shear wave velocity (Borcherdt, 1994)

Site Class or Soil Profile Type	Description	Shear Wave Velocity $\overline{V}_S$ Top 30m (m/sec)	Standard Pen. Resistance $\overline{N}$ or $\overline{N}_{ch}$ (blows/ft)	Undrained Shear Strength $\overline{S}_u$ (kP_a)
S1 A	Hard Rock	> 1500	—	—
S1 B	Rock	760 - 1500	—	—
S1 and S2 C	Very dense soil/soft rock	360 - 760	> 50	> 100
S1 and S2 D	Stiff soil	180 - 360	15 - 50	50 - 100
S3 and S4 E	Soft soil	< 180	< 15	< 50
S3 and S4 F	Special soils requiring site-specific evaluation	—	—	—

Figure 2.4 Comparison previous and new site classification code regulations (Borcherdt, 1994)

2.2 One-Dimensional (1D) Site Response Analysis (SRA) Methods

The solution of site-specific dynamic response analysis is a complex phenomenon. Different model approaches can be used for one, two, and three dimensional. The generic wave pattern (source, path), dynamic soil properties, and geometry of the base increase this complexity. Some assumptions and boundary conditions are needed to reduce this complexity or to solve the problem more quickly for SRA. These assumptions and boundary conditions of the one-dimensional site response analysis method include that groundwater level is horizontal, the soil deposits are extended horizontally, and the soil stratified are homogenous. SH waves produced vertically from source affects soil layers. Dimensional of soil stratified are infinite (Kramer, 1996).

A wave motion caused by fault rupture passes through soil layers with different propagation velocities and reaches the surface by reflection and refraction. When wave motion from a layer with a high propagation velocity passes to a layer with a lower propagation velocity, it reflects. It propagates in a more vertical direction., as illustrated in Figure 2.5. It shows that the assumption that vertical travel vertically is reasonable in many cases SRA.

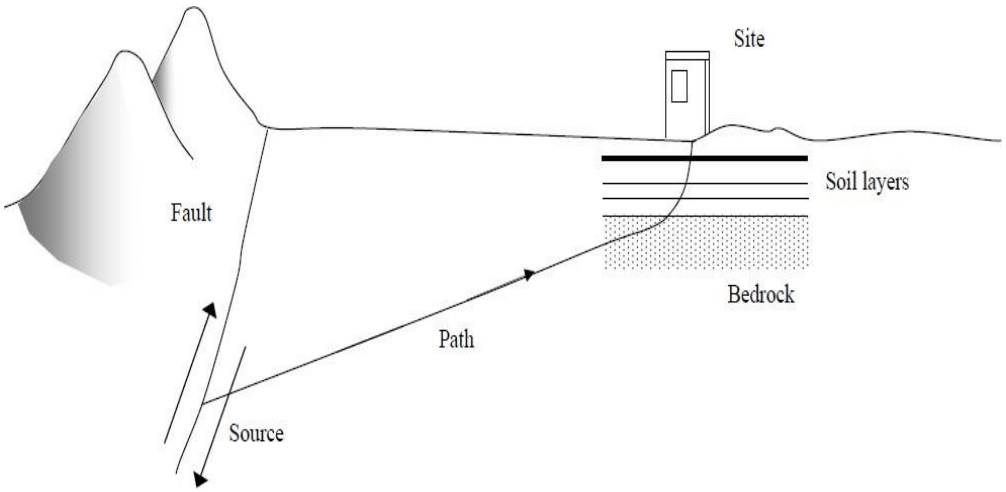


Figure 2.5 Propagation of seismic motions from bedrock to surface (Kramer ,1996)

2.2.1 Equivalent Linear (EL) Analysis Method

Seed (1972) developed equivalent linear analysis model for adjusting non-linear soil behavior. The SHAKE software (Schnabel et al., 1972) used to implement this method. The EL analysis method assumes shear modulus and damping ratio with an iterative approach as an average value for each soil deposit, as shown in the Figure 2.6.

The EL method performs operations in the frequency domain. The acceleration time records obtained from stations are convert to frequency domain via a Fast Fourier Transform (FFT). FFT separates records as the sum of the sine and cosines harmonic amplitude components. Transfer functions are then multiplied by the Fourier series to account for the effect of the soil profile's stiffness, damping, and density properties on each frequency of the base motion. This results in the Fourier series of the output motion, which is analyzed for each harmonic. The analysis results are calculated for each harmonic, and then the reverse FFT is applied to obtain the outputs in the time domain (Kramer, 1996). The equivalent linear analysis is limited in that it only considers the total stress and cannot accurately model excess pore water pressure generation and permanent deformations.

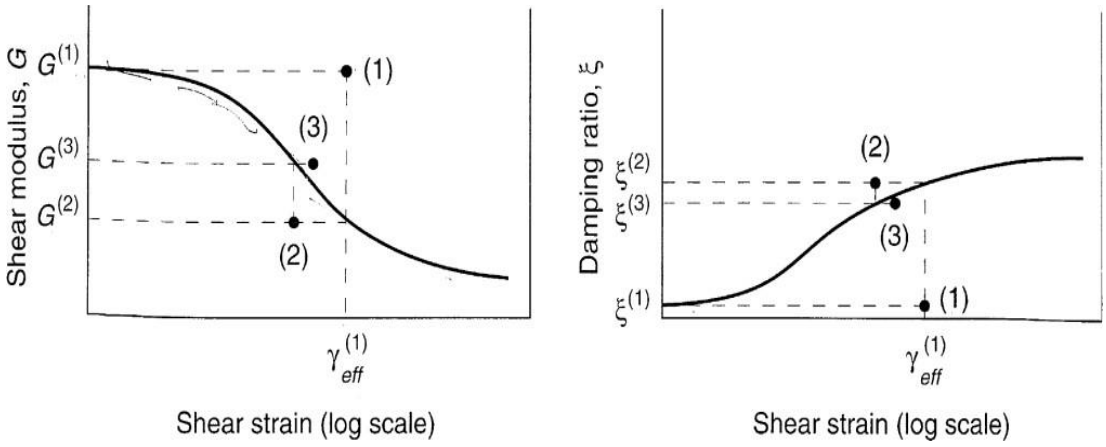


Figure 2.6 Iterative procedure in equivalent linear analysis method

2.2.2 Nonlinear Analysis Method

Soil deposits exhibiting nonlinear stress-strain behavior and pore water pressures can occur to soil due to degradation of stiffness during strong ground motion. Nonlinear analysis methods are needed because the EL analysis model assumes the dynamic properties of soils as average values and cannot produce excess pore water pressure. The DEEPSOIL wave propagation software uses the lumpy mass system to solve cyclic nonlinear stress-strain behavior. A corresponding mass, nonlinear spring, and dashpot in the lumped mass system symbolize each soil deposit. Cyclic nonlinear stress-strain relationship in one dimensional model follows the stress-strain relationship by stress path all-over the soil profile during dynamic loading, and based on extended masing rules, stress-strain paths follow each other in the loading, unloading and reloading stages, as illustrated in the Figure 2.7. The nonlinear model, using time domain solution method, changes the all over site profile's shear modulus and damping values during the during the seismic event. DEEPSOIL performs two subdivision methods, namely linear time-domain interpolation and zero padded frequency domain interpolation (Deepsoil manual, 2016). The one-dimensional cyclic nonlinear model is divided into two effective and total stress-based parameters.

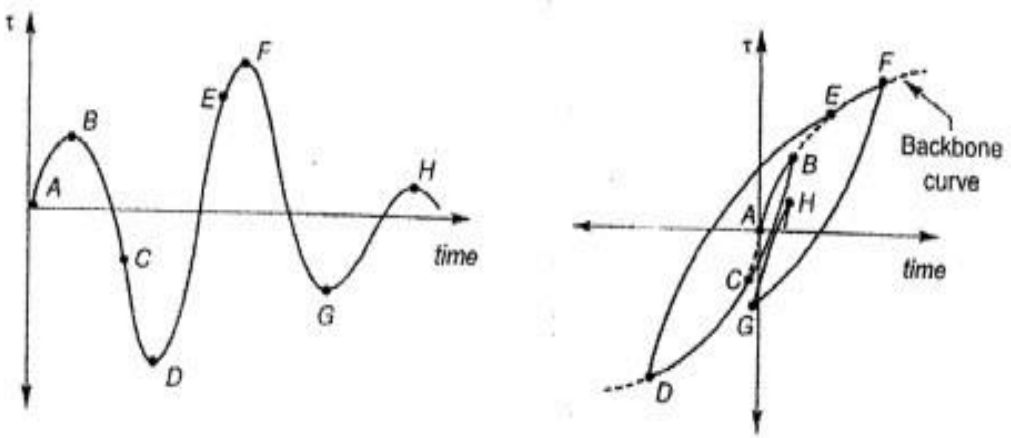


Figure 2.7 Dynamic soil response (stress-strain path) according to extended Masing rules (Kramer, 1996)

2.3 Dynamic Soil Properties

Monotonic and cyclic dynamic loadings are generally irregular, rapid, and fast. Laboratory experiments and numerical methods can be used to determine the soil's skeleton excitation response to dynamic oscillations. The cyclic event's two main dynamic soil properties are shear modulus and damping. It is recognized that the deformation behavior of the soil is highly nonlinear, revealed in the shear modulus and damping, which are affected importantly by the amplitude of cyclic strain during seismic event, soil type, and properties of main characteristics of ground motion. (Ishihara).

Determining of which properties affect shear modulus and damping ratio changing is crucial in site-specific response analysis. The most broadly used laboratory devices are cyclic triaxial shear, simple cyclic shear, cyclic torsional shear, and resonant column equipment. During dynamic loading, the tangent shear modulus determines the dynamic response of the soil skeleton, since the soil is influenced by shear waves (SH) as the soil is exposed to shear failure. As cyclic strain and the number of cycles increase, the tangent shear modulus diminishes. In contrast, the damping goes up with increasing cyclic strain and number of cycles.

In soil dynamics, concept of damping classifies as hysteresis and radiation damping. Site response analyses are needed for hysteresis rather than radiation damping. Hysteresis damping also is called material or nonlinear damping, is the energy loss in the shape of heat due to the relative movement between soil particles during dynamic loading.

Zen et al. (1978) emphasized significant influence of plasticity on the shear modulus decrement for the first time, based on their studies on the clay specimens with various plasticity indices. When the plasticity index of clay soils goes up, the shear

modulus decrement rate decreases at a slower rate with rising cyclic strain amplitude. Zen et al. (1978) demonstrated that impact of the plasticity index on shear modulus decrement was more significant and influential than confining pressure, as shown in Figure 2.8.

Vucetic and Dobry (1991) found that if the plasticity index heightens, the shear modulus decrement curve increases and the damping curve diminishes with increasing cyclic strain amplitude. The effects of the plasticity index on the shear modulus reduction are demonstrated in Figure 2.9. Result of same impact on damping curve are demonstrated in Figure 2.10. As illustrated in Figure 2.11, the effects of different plasticity indices on spectral acceleration on the same soil profile in different dominant periods are demonstrated in Figure 2.12. It was concluded that when the plasticity index rises, earthquake motion in base is amplified at the surface Effective confining pressure does not significantly affect shear modulus reduction as the plasticity index increases.

Stokoe and Lodde (1978) show that the void ratio significantly impacted the shear modulus reduction of clays, while Isenhower (1979) shows that the void ratio had little effect on the shear modulus reduction of clays. The impact of the void ratio on shear modulus reduction of clay soil is a contentious issue. Further studies are needed.

Kokusho et al. (1982) presented that consolidation stresses do not significantly act upon the shear modulus reduction based on the studies of high plasticity soils with an over-consolidation ratio of 5 to 15. Dobry and Vucetic (1987) concluded that consolidation stresses and over consolidation ratio had no remarkable effect on shear modulus. Studies since the 1970s have emphasized that plasticity index, rather than consolidation stress history, void ratio, effective confining pressure, and frequency of loading have a dominant and strong effect on shear modulus reduction of clay soils.

Seed and Idriss (1970) have indicated that such influences as grain size, degree of saturation, and void ratio have little effect on the damping ratio and shear modulus reduction of gravel and sandy soil. Hardin & Drnevich (1972), and Seed & Idriss (1970) have shown clearly affected by the mean confining pressure and relative density. The upper and lower limits of variation of dynamic soil response of sands vary in a very narrow band, while the changing of dynamic soil response of clays is in a wide range.

Ishibashi and Zhang (1993) present formulations that calculate shear modulus reduction and variation of damping for plastic and non-plastic soils.

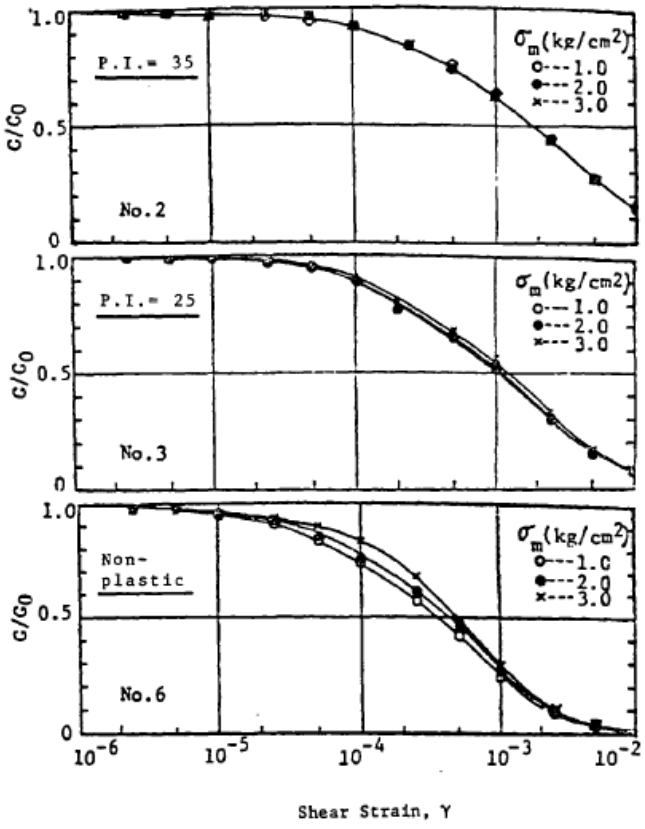


Figure 2.8 Impact of mean principal stress on shear modulus decrement relation for clays with variation of plasticity index (after Zen et., 1978)

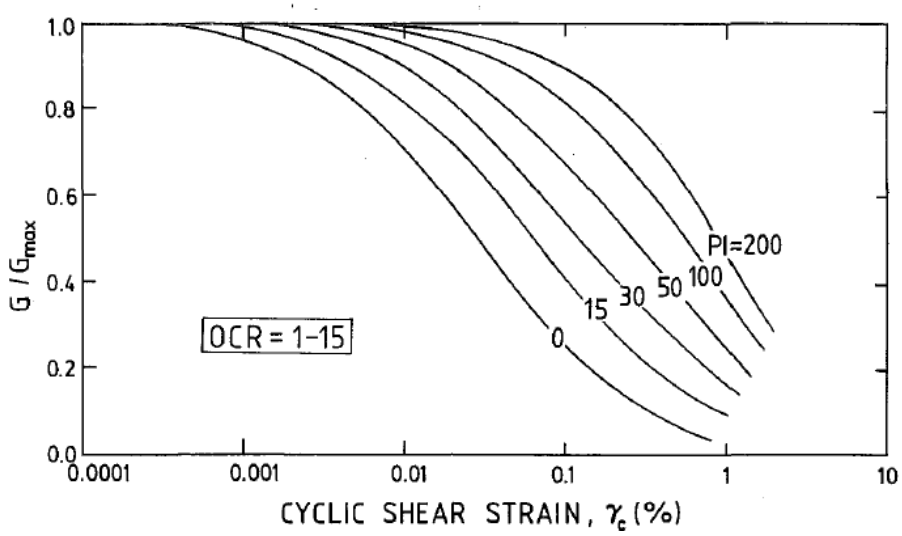


Figure 2.9 Impact of plasticity indices on shear modulus decrement with increasing strain (Vucetic, 1991)

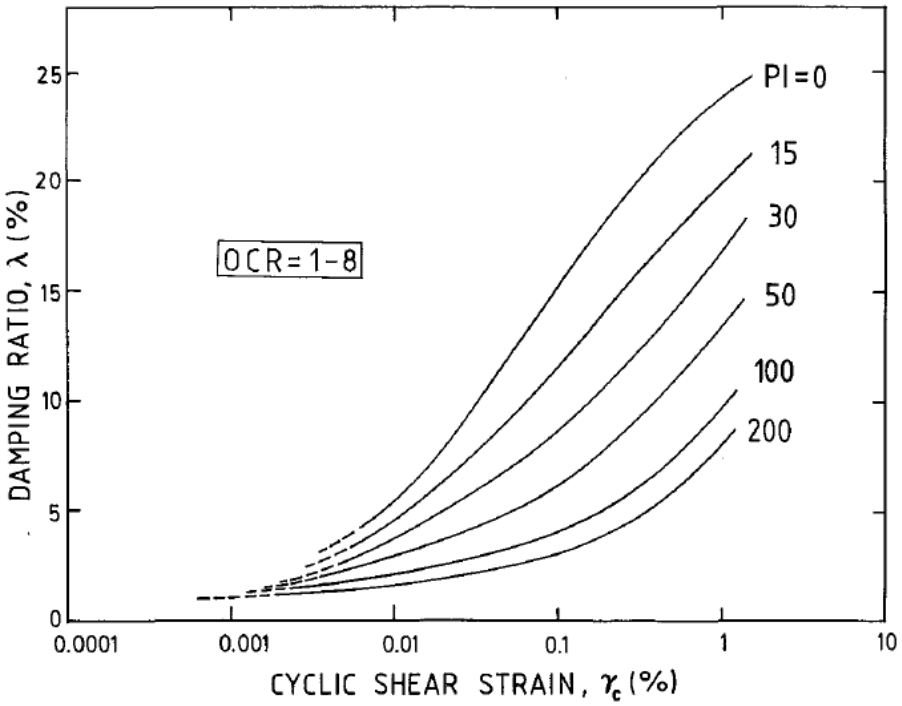


Figure 2.10 Influence of plasticity index on damping with increasing strain (Vucetic,1991)

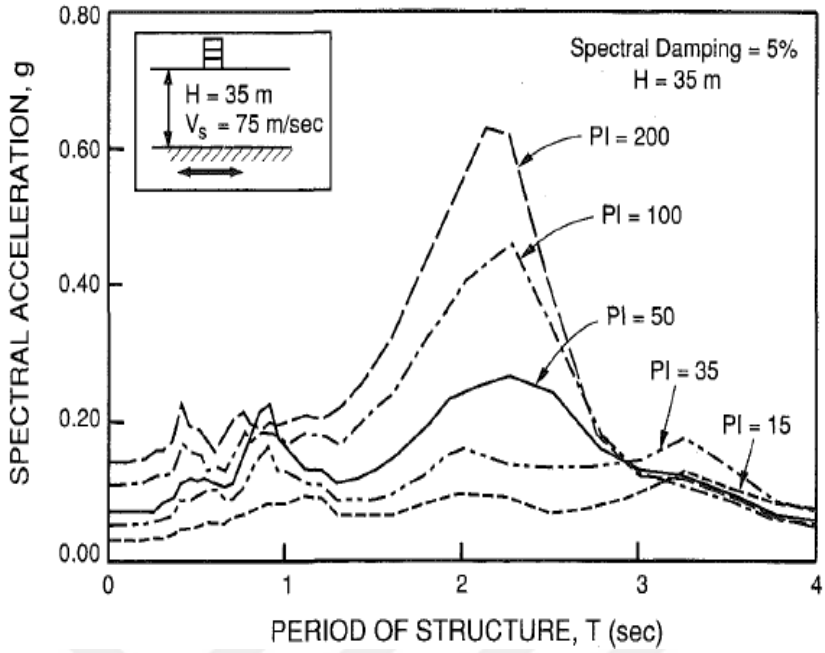


Figure 2.11 Impact of plasticity index on spectral acceleration (Vucetic, 1991)

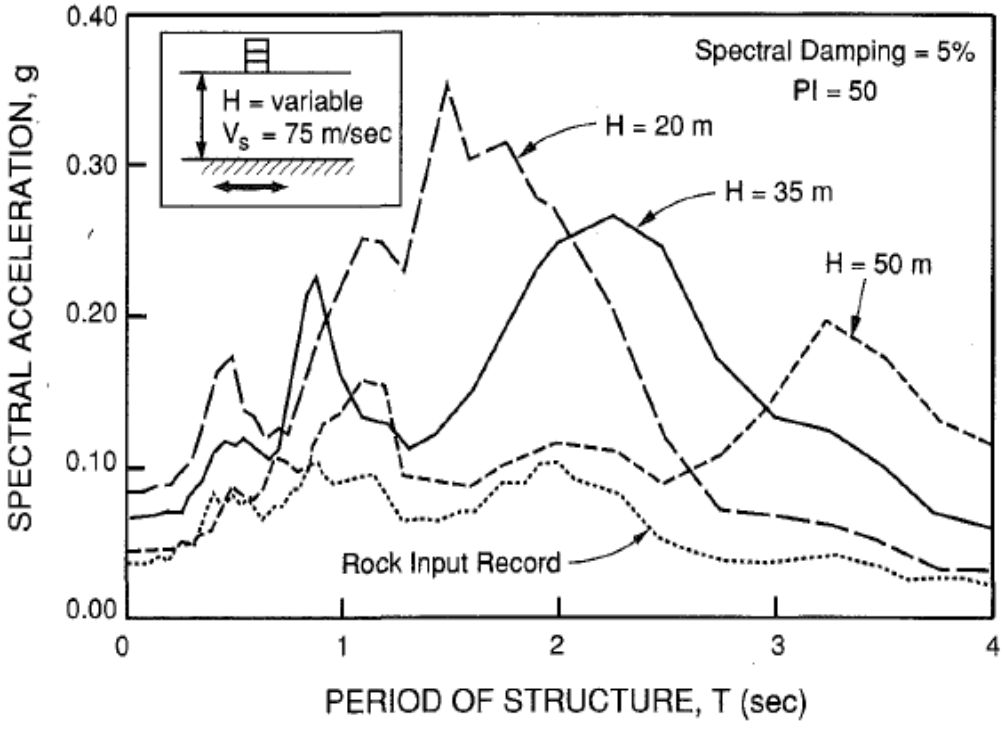


Figure 2.12 Effect of soil deposit thickness on spectral acceleration (Vucetic, 1991)

2.4 Backbone Models

To simplify the computations, the stress-strain curve is assumed to be hyperbolic. To accurately predict the spectral acceleration, deformation, shear strain, pore pater pressures, and damping ratios obtained from the site-specific dynamic soil behavior analysis results, researchers developed a suite backbone curve models that accurately calculates target shear strength, pore water pressure, damping at small strain damping, dynamic soil properties. Ramberg-Osgood and hyperbolic model establish to characterize the excitation response of the geo-material. The Ramberg-Osgood model requires more parameters more than the hyperbolic model. Developed these backbone models are used in the analyses with laboratory and numerical methods, and the accuracy of the models is revealed whether the results obtained are compatible or not. This thesis informs about models' development process of these backbone models and their implementation in deep soil software to improve the accuracy of dynamic soil behavior analysis results.

2.4.1 Modified Kondner & Zelesko (MKZ) Model

Matasovic (1993) proposed a method in that Modified Konder and Zelasko constitute to Matasovic (1993) adds to two material parameters to the original Kondner and Zelesko (1993). The Modified Kondner and Zelasko model is an abbreviated MKZ model. These material parameters B and s that obtained experimentally using curve-fitting technique. Parameters of B and s arrange the situation ordinates of shear modulus and adjust stress-stain relationship. B and s parameters vary within a very narrow range. The variation of B is from 1.5 to 1.9, while the s parameter is between 0.67 and 0.98. They are referred to as material constants due to their narrow range of variation. The Figure 2.13 shows that as parameter B diminishes with rising effective confining pressure, parameter s increases with rising mean confining pressure. The MKZ model incorporates the reduction of soil stiffness and the stress-strain relationship, as shown in equation (1). Constants B and s can be automatically determined using DEEPSOIL software to reach an optimal fit for both curves. MKZ model cannot accurately predict damping in small strains and target shear strength at

failure, as illustrated in the figure. The Figure 2.14 indicates that the MKZ model better represents nonlinear behavior of soils at small strains than the KZ model. (Matasovic & Vucetic, 1993).

$$\tau^* = \frac{\delta_G . {G_{m0}}^* . \gamma}{1+\beta(\frac{\delta_G . {G_{m0}}^*}{\delta_\tau . \tau_{m0}{}^* |\gamma|})^s} \tag{2.1}$$

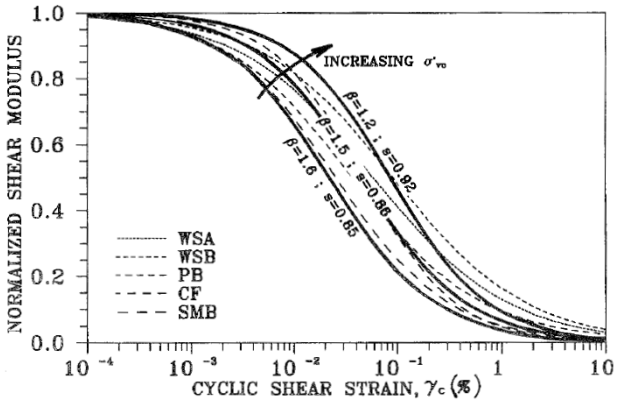


Figure 2.13 Variation of parameters B and s with increasing effective confining pressure (Matasovic & Vucetic, 1993)

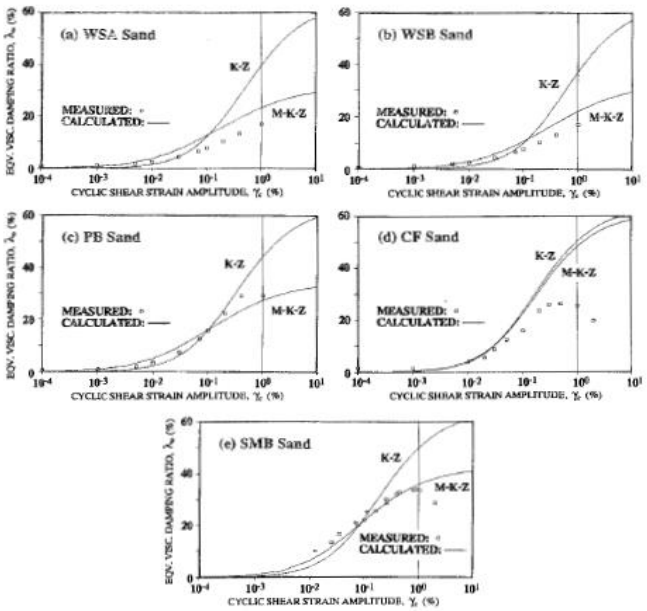


Figure 2.14 Comparison of MKZ and KZ model (Matasovic & Vucetic, 1993)

Hashash and Park (2001) suggested a original expression that considers the effect of mean confining pressure on the shear modulus decrement. It incorporates it into the MKZ model. A new expression is shown in equation 2.2 as follows:

$$\gamma_r = a(\frac{\sigma'_v}{\sigma_{ref}})^b \quad (2.2)$$

where a and b correspond to curve fitting parameters, respectively, and parameters and correspond to vertical effective confining pressure.

Hashash and Park (2001) suggested a new formulation that considers the effect increasing confining pressure on small strain damping and incorporates it into the MKZ model. A new formulation is shown in equation 2.3 as follows:

$$\delta = \frac{c}{(\sigma'_v)^d} \quad (2.3)$$

where c and d correspond to curve fitting parameters, respectively, parameter correspond to vertical effective confining pressure.

Although laboratory studies show that the damping of the soil is zero in very small strains, it is known that the soil has damping even in very small strains. In the 1985 Mexico City earthquake is an example of how low damping in small soil strains can lead to amplified weak ground motion in soft soil layers with impedance differences. Therefore, in machine foundations and other important projects, needs to account for the damping at small strains and the variation of this damping at small strains (Vucetic, 1991). To account for small stain damping, Park and Hashash (2004) suggested small strain (viscous) damping. The small strain (viscous) damping is based on an extended

Rayleigh scheme using various modes in Figure 2.15 and is automatically incorporated into the DEEPSOIL software.

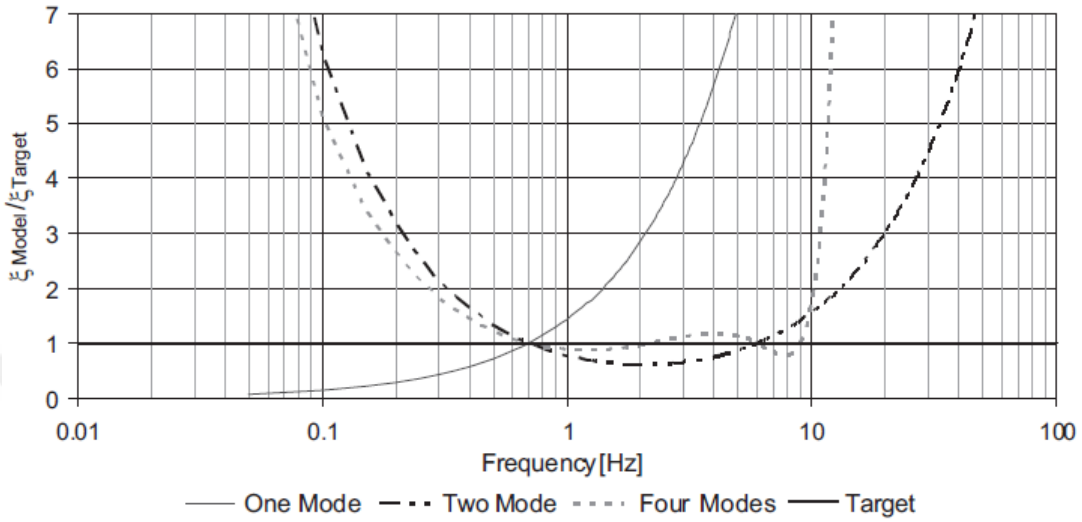


Figure 2.15 Variation of viscous damping using Rayleigh damping formulation according to period and frequency

2.4.2 General Quadratic Hyperbolic (GQ/H) Model

MKZ model cannot accurately represents target shear strength and nonlinear stress-strain. There is a solution needed to fundamentally accurate soil strength at failure and large strains. Groholski & Hashash (2016) have suggested GQ/H model that adjusts the nonlinear stress-strain behavior of soil and accurately estimates shear strength at large strains. GQ/H model suggests that θ_τ curve fitting parameter that defines the relation among normalized shear strain functions, shear strain, and shear modulus, allowing the soil to exhibit elastic-plastic behavior. Figure 2.16 shows that the GQ/H model offers more consistent results than the MKZ model.

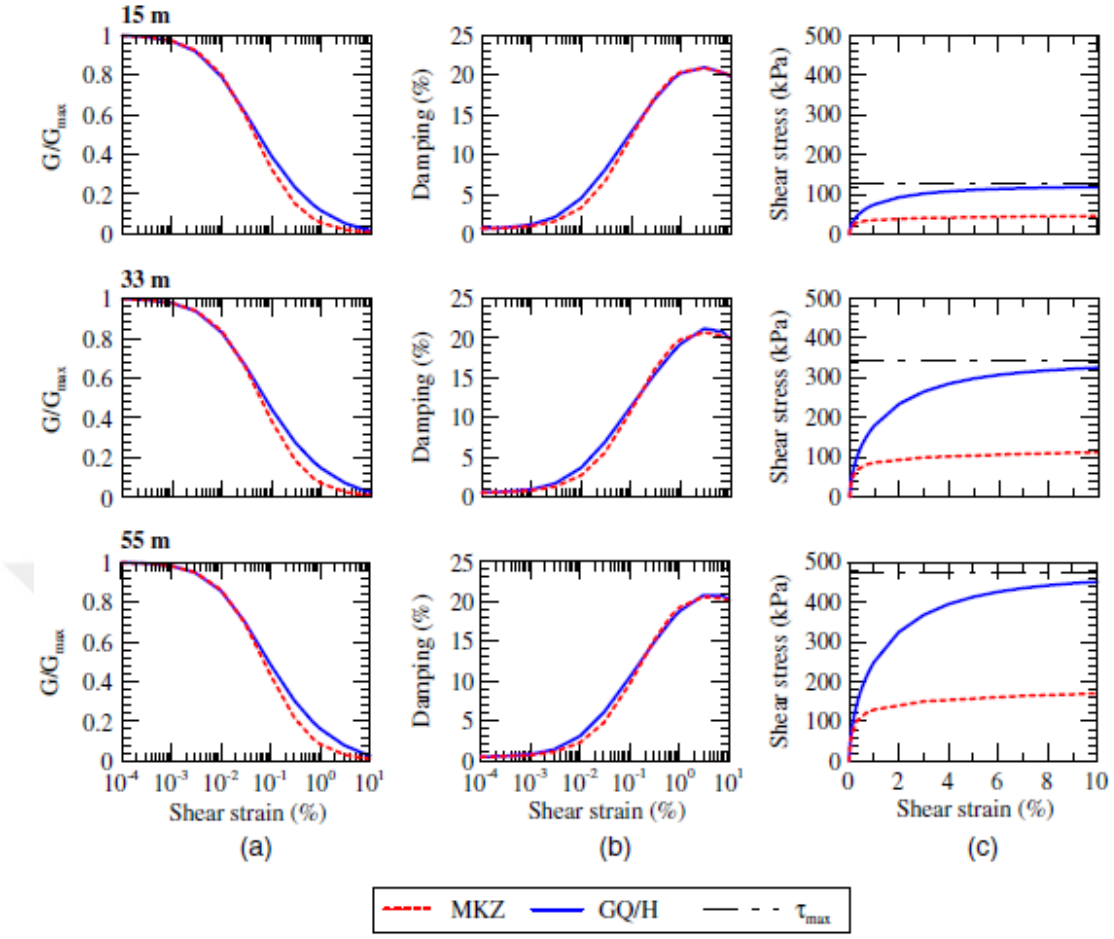


Figure 2.16 Comparison of the dynamic response of soils of different depths for different soil models in the Meoland site (Groholski and Hashash, 2016)

Another problem in soil dynamic is to simultaneously match the overestimated damping reduction at large strains with the reduced damping to the shear modulus attenuation curve. Seed (1986) and Stokoe (2004) compared the damping obtained from the test results with the damping obtained from the extended massing rules and revealed a significant difference between the two results, as illustrated in Figure 2.17. To eliminate this difference, the researchers proposed new method using an equation 2.4 to reduce damping at large strains. This method is referred modulus reduction damping reduction factor (MRDF). In equation 2.4, p_1, p_2, p_3 are curve fitting parameters. The secant and maximum shear modulus correspond to G_{γ_m} and G_0. Figure 2.18 shows that the MRDF method offers more consistent results than the methods proposed by other researchers.

$$F(\gamma_m) = p_1 - p_2(1 - \frac{G_{\gamma m}}{G_0})^{p_3} \quad (2.4)$$

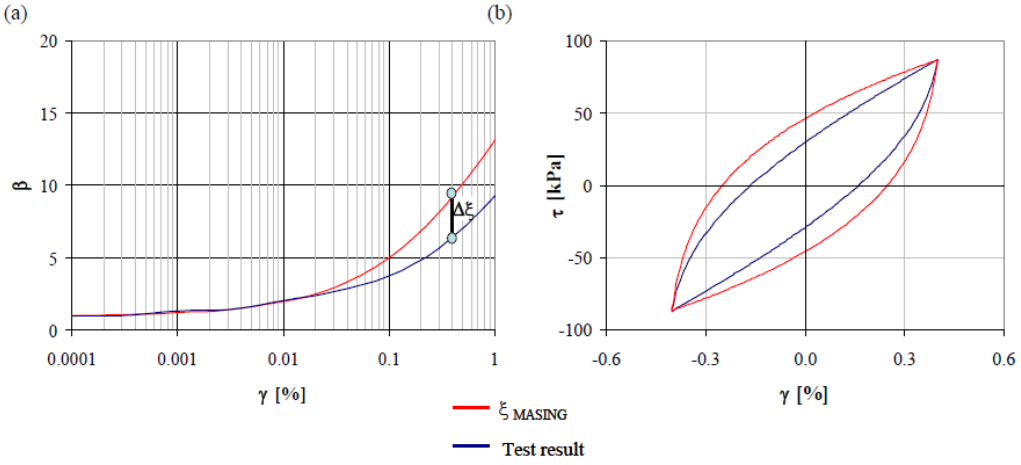


Figure 2.17 Comparison of damping ratio obtained masing rules and test result (Philips & Hashash, 2008).

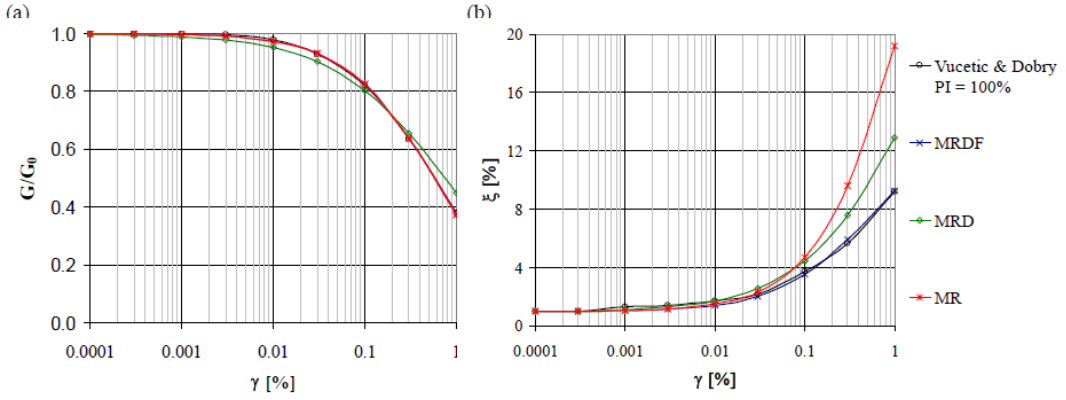


Figure 2.18 Comparison the relation of shear modulus reduction (a) and damping (b) according to different models (Phillips & Hashash, 2008)

The hysteresis loop formed during a dynamic event consists of different backbone curvatures. Applying the MRDF method correctly to each backbone curve is challenging and complex. Therefore, Hashash (2018) proposed a generalized non-masing hysteresis model method to eliminate this difficulty and complexity. Therefore,

Hashash (2018) proposed a generalized non-masing hysteresis model method to eliminate this difficulty and complexity. In this model, the loading-unloading steps of soils exhibiting elastic-plastic behavior are based on the loading surface-based kinematic stiffening plasticity law, as shown in Figure 2.19, by reducing the size of the loading-unloading steps. As a result of these processes, Hashah (2018) presented a new method that can formulate the loading-unloading parts of each backbone curve. the Figure 2.20 shows that the new model gives more accurate results than the massing-hysteresis model.

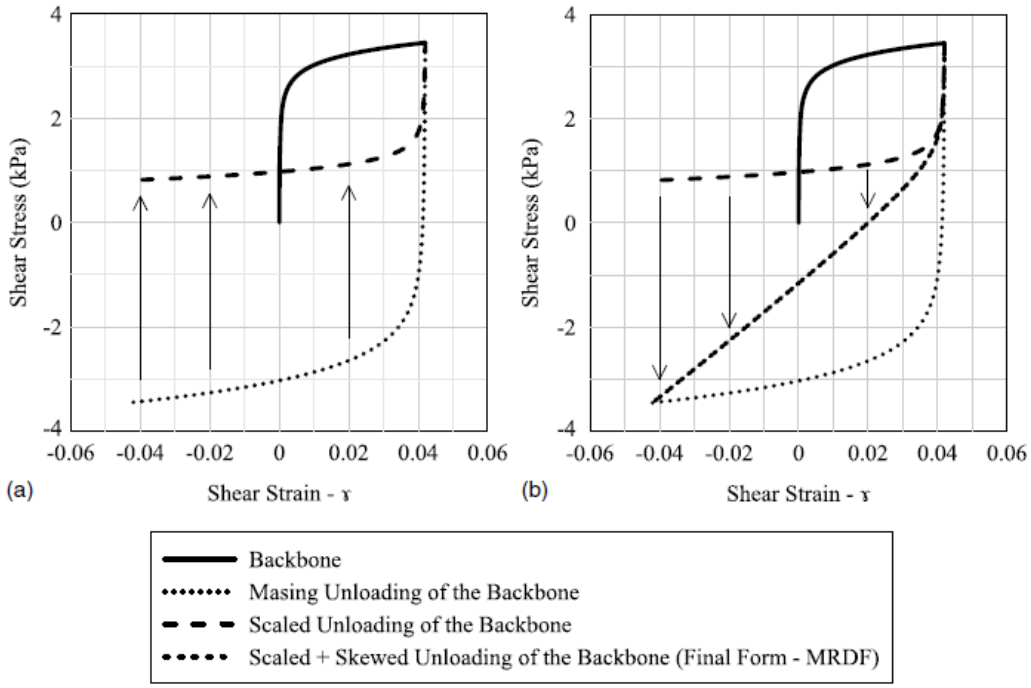


Figure 2.19 The methodogly for occuring the Generalized Non-Masing Hysteresis Model (Hahshas et al.,2017)

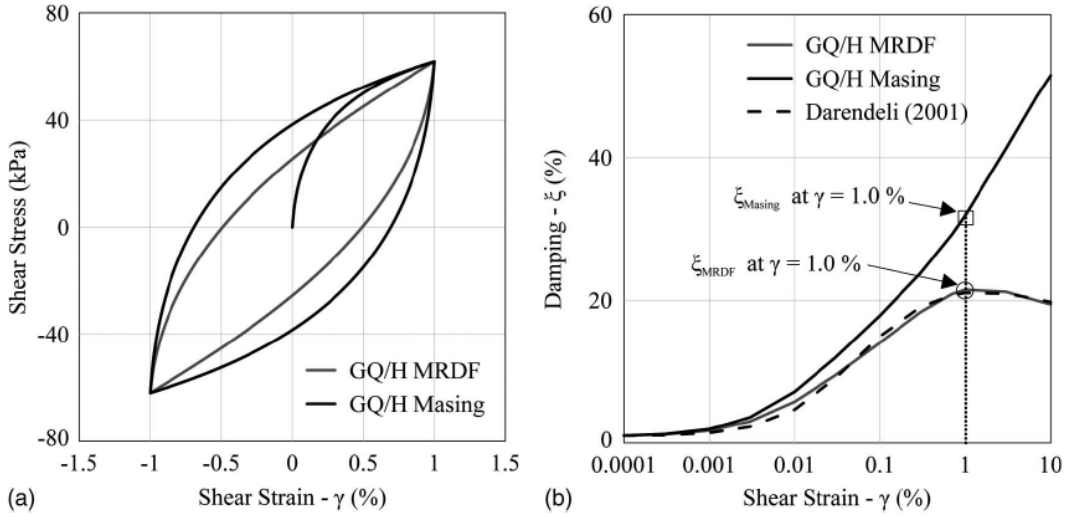


Figure 2.20 Comparison of Darendeli (2001) reference curve, Generalized Non-Masing and Masing Hysteresis Model (Hashash et al., 2017)

2.5 Excess Pore Water Pressure (PWP) Generation Models

Extensive research on the liquefaction and softening of soil phenomenon began, as Niigata, Japan, Anchorage, and Alaska earthquakes caused extensive damage. After earthquakes, these studies include field observations, development of experimental and computational methods, specifying of dynamic response of liquefiable soil deposits, investigation of mechanism of liquefaction phenomenon, and simulation. Excess generation methods were developed and combined into numerical software, after long studies. The excess pore water pressure generation in one (1D) dimensional cyclic nonlinear effective-stress-based model is divided into three classification stress-based, strain-based, energy-based model, respectively. This section informs about strain-based models. Modeling of the mechanism of excess pore water generation in saturated soft and deep saturated soil deposits cyclically sheared in undrained conditions plays a key role because of the excess pore water pressure generates, that eventually leads to decreasing shear strength and shear modulus of soil.

2.5.1 Matasovic and Vucetic Model for Clay

Although the PWP generation mechanism of normal consolidated (NC) and over consolidated (OC) clays is theoretically like that of sands. The pore water production mechanism of typical clays, especially OC clays, is more complicated than sands. The first reason is related to the microstructure of the clays. The second reason is that when OC clays produce negative pore water pressure, the shear modulus of OC clays decreases due to degradation despite the increase in effective stress. This phenomenon conflicts with the effective stress principle. This conflict shows that degradation is not the only impact on the excess PWP of clays as in sands. (Vucetic,1987)

A new excess PWP generation model that generates for clay soil are proposed by Matasovic & Vucetic (1993). A model of generation excess PWP and reduction of stiffness clay was developed by performing cyclic controlled experiments on Venezuelan offshore marine clay, abbreviated VPN clay. Pyke (194, 1985) proposed a hyperbolic equation representing the degradation parameter (t) of soil stiffness, depending on the relationship between cyclic strain, volumetric threshold strain, and curve-adjusting parameters s and r. Degradation parameter t is established by $s(\gamma_c - \gamma_{tv})^r$ equation of 2.5. Parameters s and r are the functions of the plasticity index and over-consolidation ratio, as illustrated in Figure 2.21 for VNP clay. Figure 2.22 shows that influence of over-consolidation ratio and number of cycles on degradation parameter. The equation 2.6 shows the general mathematical form of the model. The model was developed as a curve fitting technique, and over consolidation ratio, threshold strain, cyclic strain, and the number of cycles is the mathematical functions of the model. Dimensionless one soil parameter and six curve fitting parameters are respectively volumetric threshold strain (γ_{tv}), A, B, C, D, s, r for VNP clay. A, B, C, and D parameter values change depending on the over-consolidation and the number of cycles, as illustrated in Figure 2.22.

$$\delta = N^{s(\gamma_c - \gamma_{tv})^r} = N^t \tag{2.5}$$

$$u = AN_c^{-3s(\gamma_c-\gamma_{tv})^r} + AN_c^{-2s(\gamma_c-\gamma_{tv})^r} + CN_c^{-s(\gamma_c-\gamma_{tv})^r} + D \qquad (2.6)$$

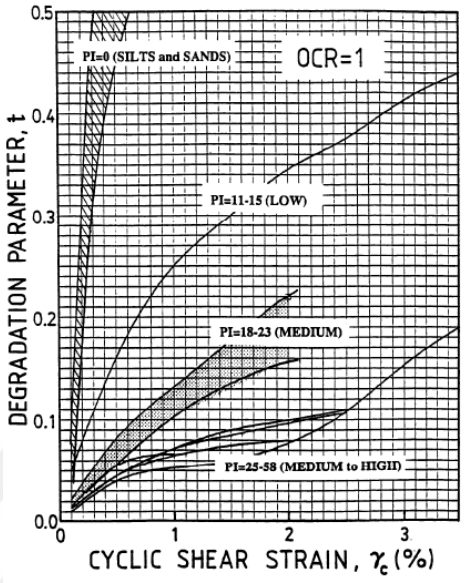


Figure 2.21 Variation of the t parameter depending on plasticity index (Tan and Vucetic 1989; Vucetic 1994).

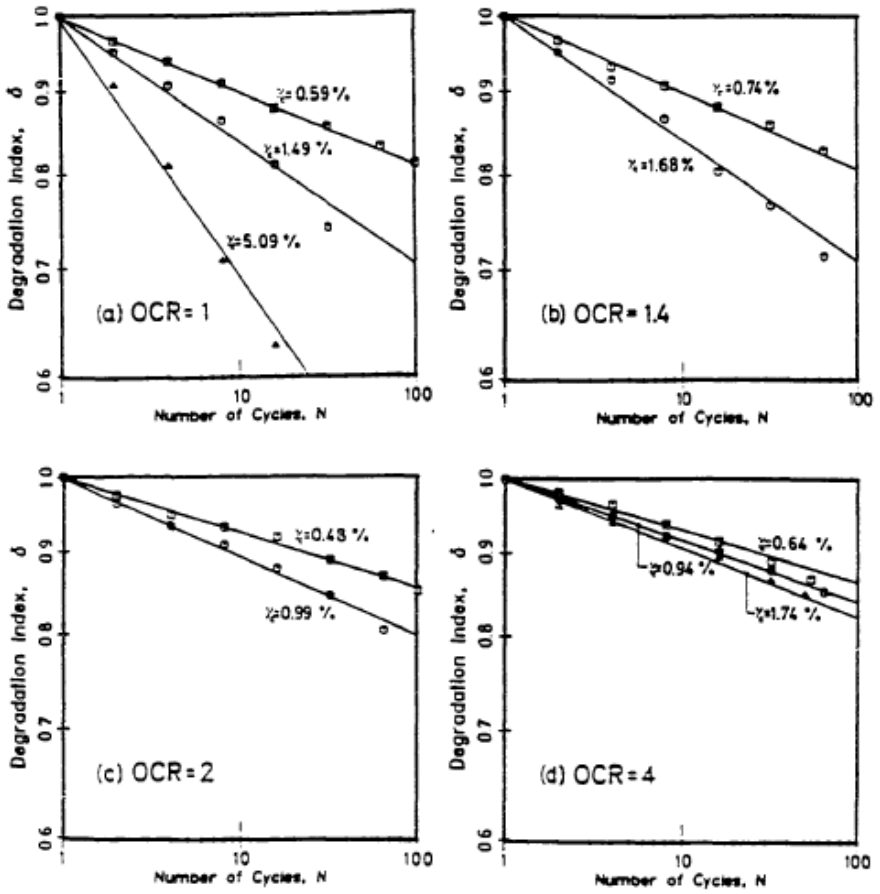


Figure 2.22 Impact of over-consolidation ratio and number of cycles on degradation index (Vucetic and Dobry, 1988; Vucetic, 1988)

2.5.2 Dobry/Matasovic Model for Sand

Dobry (1987) proposed a new pore water generation model using strain-controlled test devices in different laboratories at different densities, not connected to the fabric of the samples. Model was incorporated DESRAMOD software. The model shows that the experimental results and the analysis results conducted with DESRAMOD the software are compatible with each other. Also, during dynamic loading in the model, the PWP generation mechanism in the site profile and loss of the produced excess PWP are provided to work simultaneously. Equation 2.7 indicates the mathematical operating principle of the new model, which generated excess pore water pressure.

$$\int_0^u \frac{du}{E_r(u)} = n_c g(\gamma_{cy}) \quad (2.7)$$

The model was developed as a curve fitting technique, and shear wave velocity, threshold strain, cyclic strain, shear wave velocity, fines content and the number of cycles is mathematical functions of the model. Dimensionless one soil parameter, one parameter loading direction and three curve fitting parameters are respectively volumetric threshold strain (γ_{tv}), p, f, F, N, s for Heber Road and Wildlife sands samples. Equation 2.8 shows final form of model.

$$u_N{}^* = \frac{p.f.F.N.(\gamma_c - \gamma_{tvp})^s}{1 + f.F.N.(\gamma_c - \gamma_{tvp})^s} \quad (2.8)$$

Empirical correlations of Carlton (2014) were used that excess pore water pressure parameters F and s for sands, as shown equation 2.9, 2.10.

$$\mathrm{F} = 380 * \mathrm{V_s}^{(-1.55)} \quad (2.9)$$

$$\mathrm{s} = (\mathrm{FC} + 1)^{0.1252} \quad (2.10)$$

With her experiments on sands using resonant-column experiments, Iwasaki (1977) suggested that the shear modulus of sands decreases as the uniformity coefficient decreases. It showed a logical relationship between the coefficient of uniformity, relative density, and shear wave velocity for sand soils could be established. Hashash (2015) conducted stress-controlled experiments to evaluate the relationship between the coefficient of uniformity and shear wave velocity and the impact of this relationship on the pore water generation mechanism and then translated these experimental results into deformation-controlled experiment results. Hashash (2015) compared the results of this experiment with Kenan's studies (2005) and showed that the results obtained gave good results, as seen in Figures 2.24, 2.25. In addition, Seed's

studies (1988) on Mexico City clay showed that the calculated surface accelerations change even with minor changes in shear wave velocity, such as 10%. It is another example of the importance of shear wave velocity in calculation results.

Based on his experiments and calculations on Santa Monica Beach (SMB) sand, Matasovic (1995) showed that the value of v=3.8 for the excess pore water formation mechanism is more consistent with the results of the experiment and calculation, compared to the value of v=1 for PWP generation when (a) and (b) in Figure 2.23 are compared.

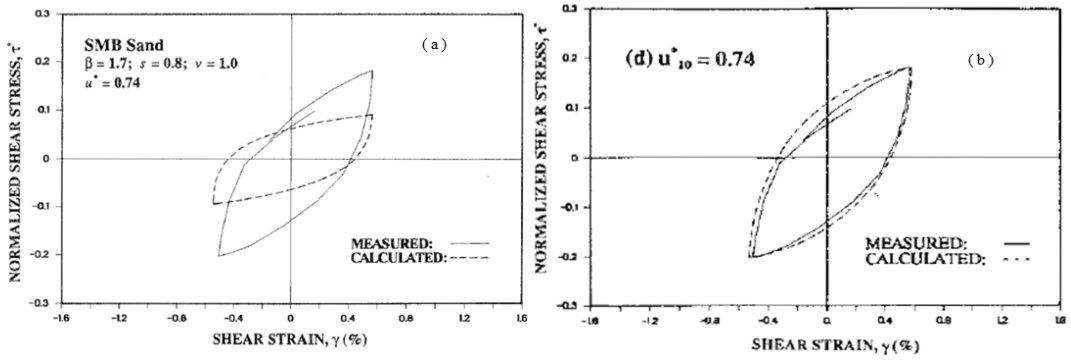


Figure 2.23 Comparison of laboratory determined and calculated PWP generation: (a) v=1; (b) v=3.8

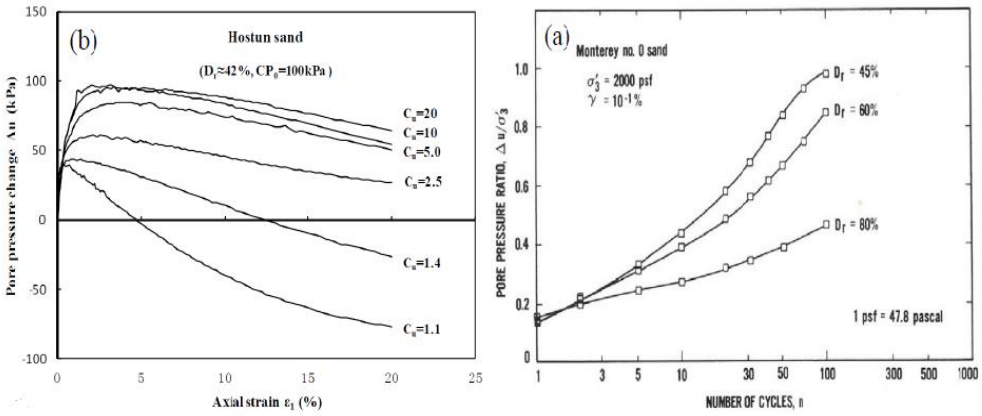


Figure 2.24 (a) Influence of Dr on PWP mechanism (Dobry, 1982); and (b) effect of Cu on PWP mechanism (Li, 2013)

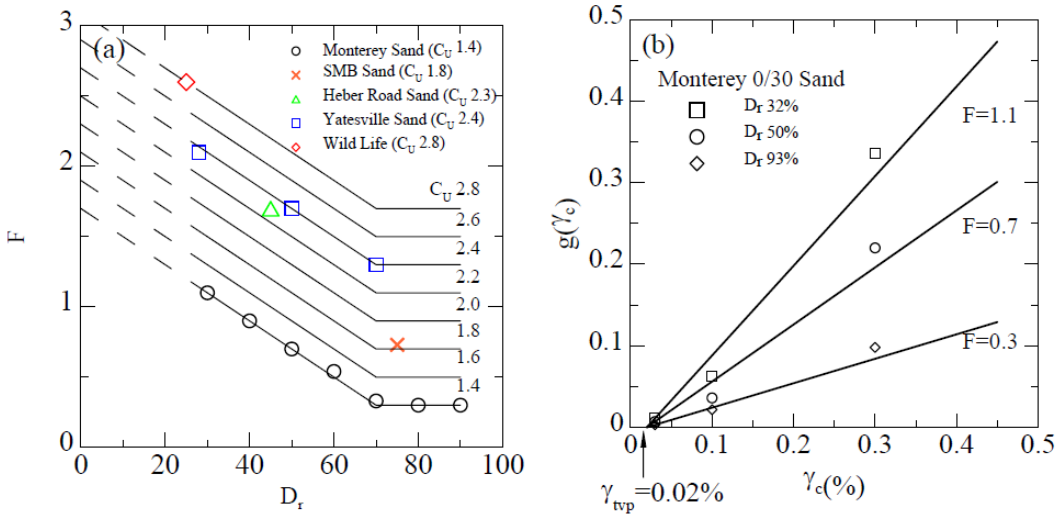


Figure 2.25 (a) Suggested relationship to predict F coefficient; and (b) comparison of relation reproduced from stress-based experiments with data from strain-based experiments from Kenan (2005)

CHAPTER 3

ANALYSIS METHOD AND PROPERTIES OF SITE CHARACTERISRICS

3.1 Analysis Method

In model has been used cyclic nonlinear effective stress-based analysis type that can perform in terms of effective stress, PWP generation redistribution, dissipation. One (1D) SRA has been performed as nonlinear effective stress-based approaching using in the time domain solution method. Time-domain solution method, the separated soil deposit is corresponded via multiple degrees of freedom lumped parameter models occurring of spring-mass-dashpot systems. Time-domain solution method permit seismic site response like shear modulus and damping within a specified layer to vary with throughout as the strains varies in the soil deposit. The soil model was selected as the GQ/H model. The model's unload-reload rules and coupling with excess PWP mechanism are also suggested in nonlinear SRA to solve for the dynamic response of multi-degree-of-freedom systems exposed to input oscillation. Depended on the formulation suggested by Darendeli (2001), the modulus reduction and damping curves for each of the soil layers were acquired. This operating establishes according to plasticity index, over consolidation ratio, number of cycles, confining pressure, and angle of internal friction. Thereafter, dynamic response curves were adjusted via the MRDF calibration method (Phillips and Hashash, 2009) to describes θ parameter for the dynamic response of soil at model. Bedrock has been modeled as an elastic half-space. Selected input motions were defined at 50 m to perform convolution analysis type in the DEEPSOIL model. Dissipation and redistribution of excess pore water generation during dynamic loading was adjusted via 1-D consolidation theory (Terzaghi,1925) in DEEPSOIL model. Soil layers were divided into sublayers according to 30 Hz. Non-masing Re/Unloading hysteretic model used in analyses.

3.2 Properties of Site Characteristics

The Izmir Bay area consists of deep alluvial soil deposits in a region that is prone to earthquakes, and soil deposits in area are known to be particularly susceptible to liquefaction during strong ground motion. In addition, the low and high plasticity clays in the area can also contribute to amplification of seismic waves during strong ground motion. In this study, the Bayraklı region was chosen to specify the impact of dynamic response of soil on dynamic site response. Within the scope of this thesis, analyzes were carried out on five different sites located in the Bayraklı region, named respectively D, E, Y, YG, and R. Tables 2.1, 2.2, 2.3, 2.4, and 2.5 show the characteristic soil properties of sites E, R, D, Y, and YG, respectively. The groundwater level in the sites varies between 2 and 3.5 m. The Bayraklı soil deposits are generally composed of alternating layers of sand and clay. Fines content of sand layers varies from 9% to 30%. Changing of sandy soil of region is from loose to moderately dense sands up to depth of 50 m. The plasticity index of soil layers varies range from 4 to 20. Soil properties were shown in Appendix. The fundamental period of D, E, Y, YG, and R sites are respectively 0.65 s, 0.76, 0.85, 0.8, and 0.83 s. The engineering bedrock at the sites is about 300 m in depth. All profile comprises alternating soil layers of silty sands and clays from the surface to 50 m. The average shear wave velocities of the D, E, Y, YG, and R sites in the upper 30 meters are 235,200,206,215,220 m/s, respectively. The soil class of D, E, Y, YG, and R areas is ZD according to Turkish building earthquake regulations. However, these sites correspond to the ZD class, and site-specific soil dynamic behavior shows a risk of liquefaction in the upper 20 m.

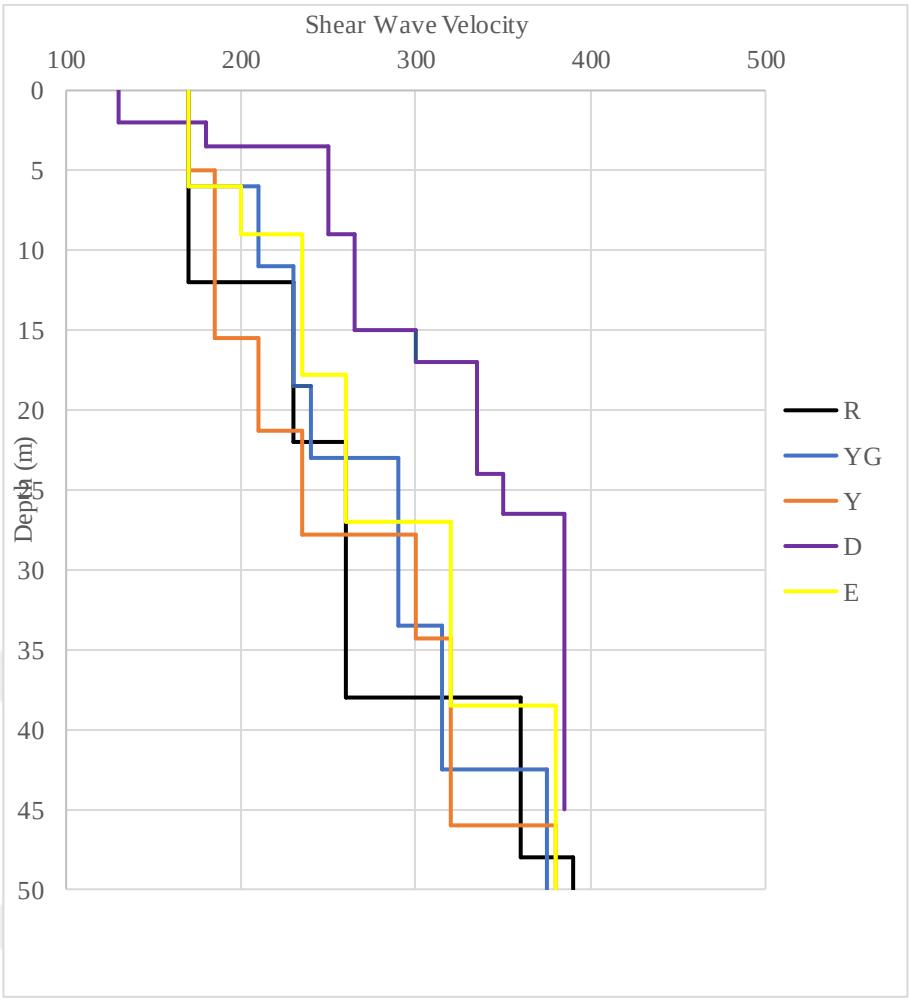


Figure 3.1 Variation of shear wave velocity with depth for five different sites

Table 3.1. Soil Properties of E Site

Layer no	Material type	Thickness (m)	Plasticity index	Fines content (%)
1	Fill	1	NP	22
2	CL	3.4	14	47.98
3	GM	4.6	NP	21.18
4	CL-ML	1.5	8	64.09
5	CL	1	18	77.65
6	CL-ML	1	8	61.32
7	GM	1.7	NP	13.01
8	CL	3.6	7	79.2
9	SM	1.4	NP	21.31
10	CL	1.8	19	69.78
11	ML	1	3	58.07
12	CL	0.7	14	46.48
13	SM	1.2	NP	21.73
14	CL	1.1	15	53.14
15	GM	2	NP	13.01
16	ML	1.4	4	52.52
17	SM	2.3	NP	25.64
18	ML	1.5	4	53.74
19	CL	1.5	20	88.54
20	SM	5.5	NP	18.33
21	ML	1.5	5	57.48
22	CL	5	20	82.96
23	GM	1	NP	21.95
24	CL	3.3	12	59.54

Table 3.2 Soil Properties of R Site

Layer no	Material type	Thickness (m)	Plasticity index	Fines content (%)
1	Fill	1.5	NP	22
2	CL	1.5	17	58.67
3	SM	1.3	NP	20.37
4	CL-ML	3.2	7	60.5
5	CL	0.5	16	48.19
6	SM	2.5	NP	21.2
7	CL-ML	4.5	7	62.39
8	GW	3	NP	9.01
9	SM	3	NP	15.11
10	CL	3	18	74.26
11	SM	1.5	NP	15.11
12	CL-ML	1.5	7	62.91
13	SM	1.5	NP	10.9
14	CL	0.5	16	47.87
15	GW	1	NP	10.9
16	ML	8	7	74.08
17	CL	7	11	77.77
18	CL	5	16	77.7

Table 3.3 Soil Properties of D Site

Layer no	Material type	Thickness (m)	Plasticity index	Fines content (%)
1	Fill	2	NP	22
2	SM	1.5	NP	47.44
3	CL	4	18	83.75
4	CL	3	13	47.68
5	SM	3	NP	24.63
6	CL	1.5	19	71.03
7	SM-GM	16.5	NP	20.19
8	CL-ML	9.5	7	78.72
9	CL	2.5	15	76.5
10	CL-ML	6.5	7	66.09

Table 3.4 Soil properties of Y Site

Layer no	Material type	Thickness (m)	Plasticity index	Fines content (%)
1	Fill	1.5	NP	22
2	CL-ML	3	6	61.96
3	CL	3	14	61.96
4	CL-ML	1.5	7	60.5
5	CL	2	17	48.19
6	ML	2.5	5	21.2
7	SM	2	NP	20.19
8	ML	3	5	60.66
9	CL	0.5	17	76.5
10	SM	2.5	NP	23.45
11	CL-ML	6	5	61.96
12	CL	3.3	14	62.91
13	SM	5.2	NP	21
14	ML	2.3	6	59.79
15	SM	2.5	NP	22
16	ML	4.2	7	62.19
17	SM	2.3	NP	20
18	CL	2	17	77.7

Table 3.5 Soil properties of YG Site

Layer no	Material type	Thickness (m)	Plasticity index	Fines content (%)
1	Fill	1	NP	22
2	CL-ML	3.5	7	58.67
3	GM	0.5	NP	17.06
4	CL-ML	2	18	67
5	GM	2	NP	19.51
6	CL-ML	3	17	70.45
7	GM-SM	5	NP	22.6
8	SC	3	12	36
9	CL-ML	6	7	82.33
10	GW-GM	6.5	NP	8.13
11	CL-ML	1.5	17	56.57
12	SM	3	NP	20.32
13	CL-ML	7	17	71.03
14	GM	1	NP	19.08
15	ML	3	4	68.41
16	CL-ML	2	16	74.08

CHAPTER 4
CASE STUDIES

4.1 Case-1 (Determination of effect of 2020 Samos Earthquake on bayraklı soils)

On October 30, 2020, an earthquake called Samos caused loss of life and damage to buildings in the Bayraklı area, 70 km from the source. In the 2020 Samos earthquake, at station 3522, the E and N components of the surface records were reduced to the soil depth corresponding to the ZC soil class type by the deconvolution method. In this part, spectral accelerations, and amplification factors (AF) are investigated and discussed using the E and N components of the recording obtained by the deconvolution method to analyze five different fields.

4.1.1 Deconvolution Method

Acceleration-time history records at rock are often unavailable in alluvial ground regions; since the bedrock level is too deep, acceleration records measured at the soil surface are taken. To calculate the SRA more reasonably via accurate acceleration records, the deconvolution method, which is the process of downloading the acceleration records from the surface to the rock or rigid soil layers, is used. Deconvolution procedure depends on using transfer functions with the equivalent linear analysis method. Silva (1988) proposed the deconvolution method, which proposes to use the surface recording in a deconvolution method of the resulting recording by first filtering all motion to the 15 Hz and reducing the amplitude of the filtered recording by 87%. The deconvolution method reduced components N and E of the station referred to 3522 to a depth representing to the ZC class.

The figure 4.1 demonstrates the idealized soil profile of the 3522 coded Çamdibi health center. Figures 4.2 and 4.3 indicate the shear modulus and damping ratio curves for clay soils. Figures 4.4 and 4.5 indicate the shear modulus and damping curves for cohesionless soils.

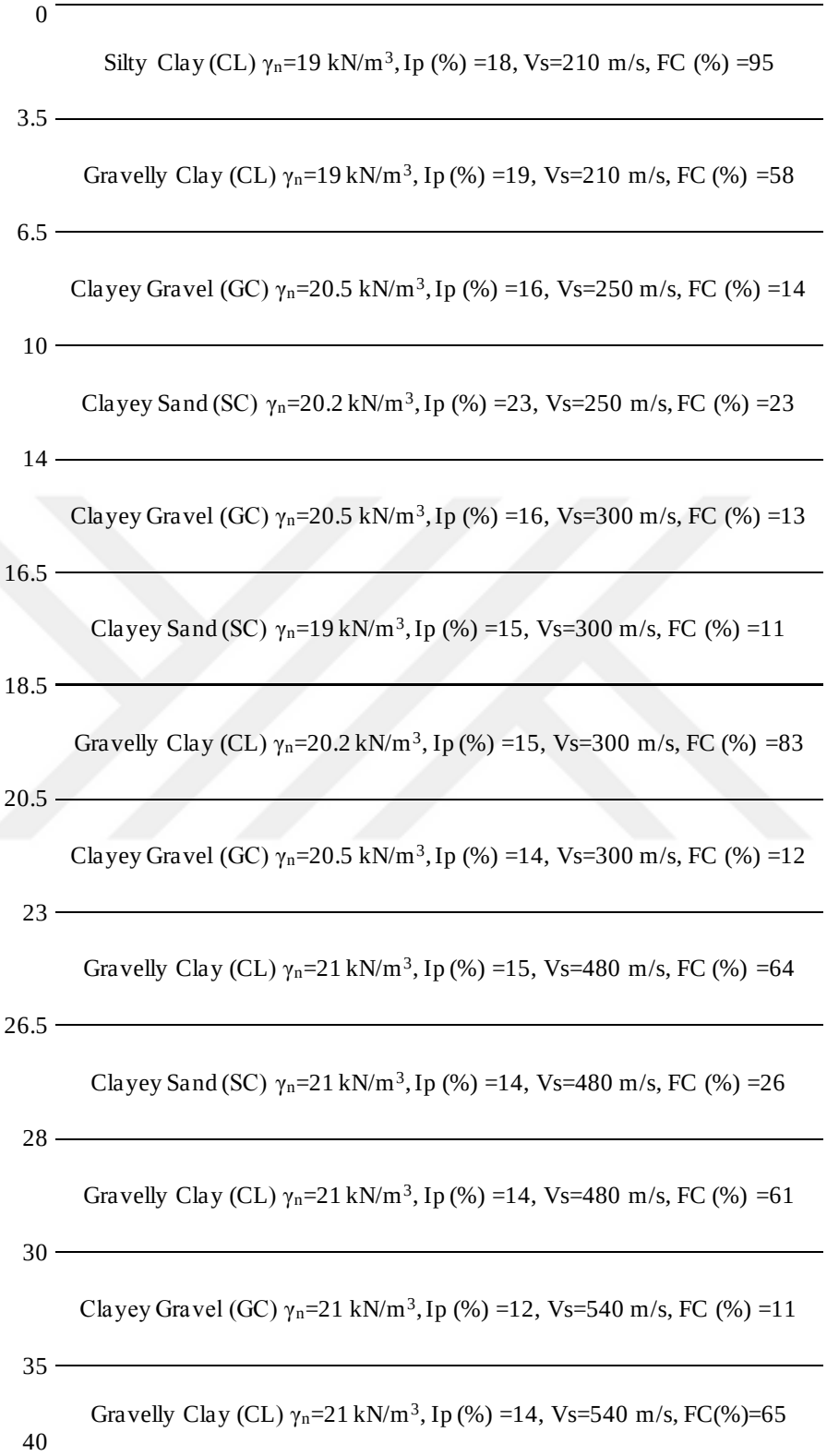


Figure 4.1 Idealized soil profile 3522 station (Altunevlek, 2022)

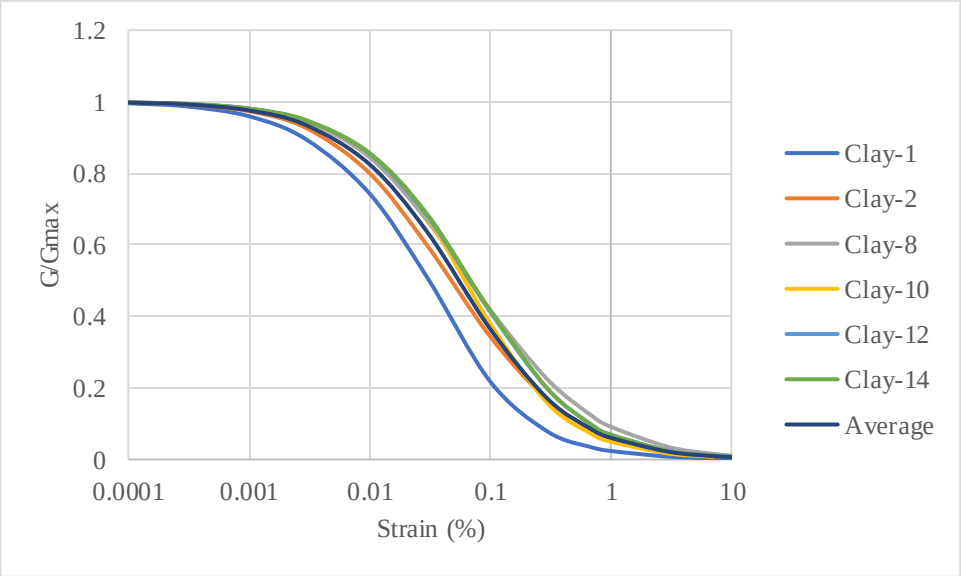


Figure 4.2 Shear modulus reduction of clay soils used in the deconvolution

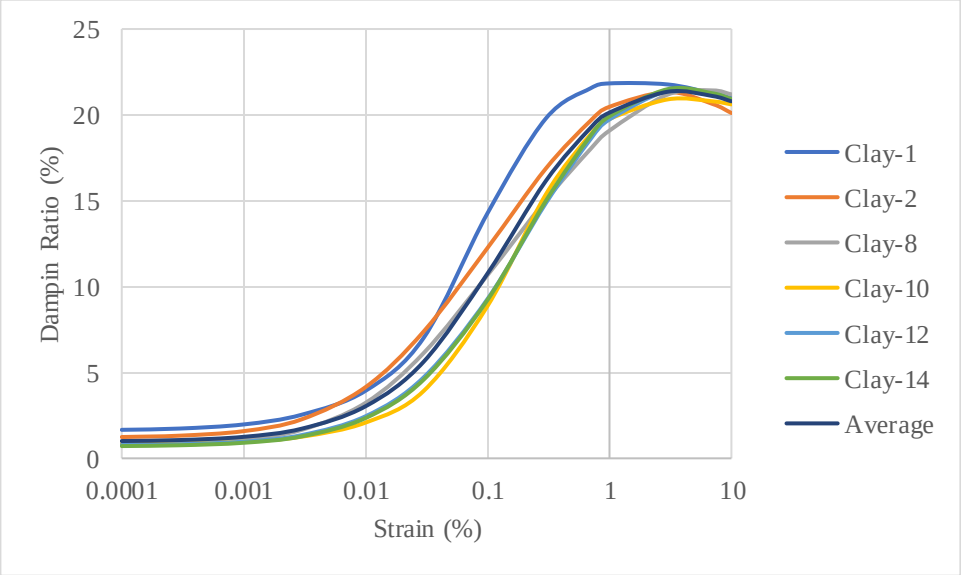


Figure 4.3 Variation of dampingratio of clay soils used in the deconvolution method

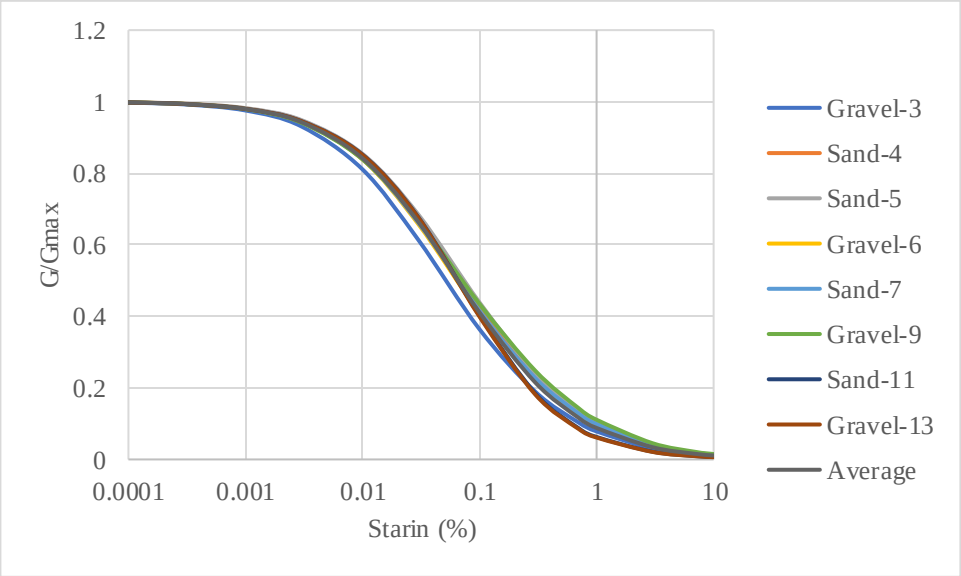


Figure 4.4 Shear modulus reduction curve of cohesionless soils used in the deconvolution method

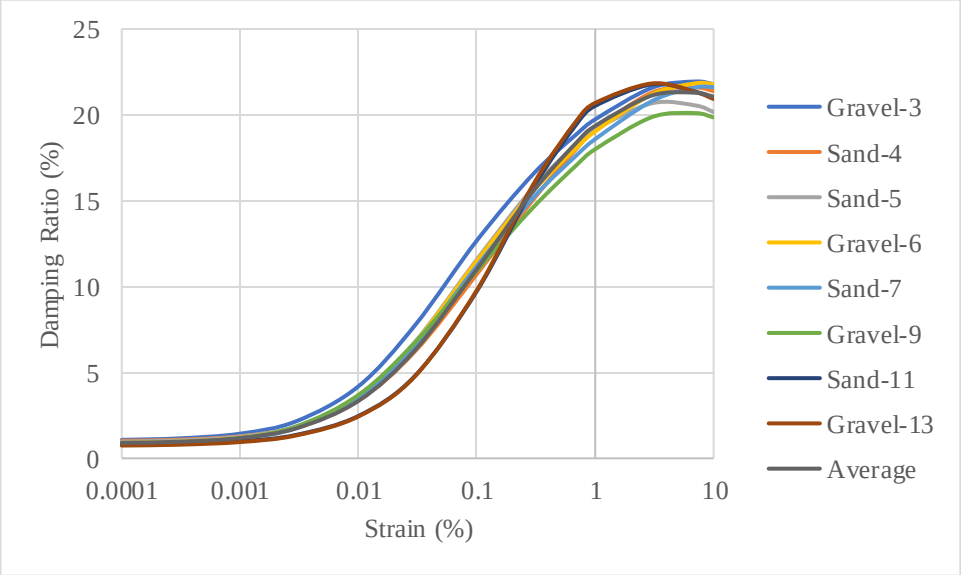


Figure 4.5 Variation of dampingratio of cohesionless soils used in the deconvolution method

4.1.2 Result of Analysis

Tables 4.1 and 4.2 show the changing of seismic soil response obtained by the deconvolution method. Figure 4.6 shows that the maximum acceleration of the e component of the surface record is 0.058g. In contrast, the Figure 4.7 shows that the ground acceleration of the e component of the record in rock is 0.04g. Figure 4.8 shows

that the maximum acceleration of the N component of the surface record is 0.075g. In contrast, the Figure 4.9 shows that the ground acceleration of the N component of the record in rock is 0.04g. Figures 4.10 and 4.12 show the spectral accelerations at the surface obtained as a result of the analyzes made using the e component in the rock at different sites. Figures 4.11 and 4.13 show the spectral amplification factor (AF) at the surface obtained as a result of the analyzes made using the e component in the rock at E, D, R, Y, and YG sites.

Table 4.1 Equivalent Linear Deconvolution analysis result for East-West direction

Layer No	**Middle of Layer (m)**	**Maximum Strain (%)**	**G/G_{max}**	**Damping (%)**	**G_{max} (Mpa)**	**Shear Modulus (Mpa)**	**γ (kN/m^3)**
1	1.75	0.0027	0.952	1.586	85.41	81.300	19
2	5	0.0082	0.875	2.598	85.41	74.766	19
3	8.25	0.0086	0.884	2.877	130.61	115.502	20.5
4	11.5	0.0123	0.854	3.359	128.70	109.926	20.2
5	13.5	0.0143	0.841	3.818	128.70	108.240	20.2
6	15.25	0.0105	0.868	3.140	188.07	163.157	20.5
7	17.5	0.0128	0.851	3.479	174.31	148.281	19
8	19.5	0.0133	0.831	3.255	185.32	154.017	20.2
9	21.75	0.0139	0.844	3.721	188.07	158.696	20.5
10	24.75	0.0053	0.915	2.119	493.21	451.195	21
11	27.25	0.0056	0.921	2.293	493.21	454.190	21
12	29	0.0059	0.905	2.229	493.21	446.573	21
13	32.5	0.0049	0.932	2.121	624.22	581.912	21
14	37.5	0.0059	0.923	2.315	624.22	576.175	21

Table 4.2 Equivalent Linear Deconvolution analysis result for North-South direction

Layer No	Middle of Layer (m)	Maximum Strain (%)	G/G_{max}	Damping (%)	G_{max} (Mpa)	Shear Modulus (Mpa)	γ (kN/m^3)
1	1.75	0.0020	0.962	1.404	85.41	82.193	19
2	5	0.0061	0.902	2.109	85.41	77.052	19
3	8.25	0.0065	0.908	2.305	130.61	118.560	20.5
4	11.5	0.0095	0.876	2.802	128.70	112.764	20.2
5	13.5	0.0112	0.862	3.025	128.70	110.939	20.2
6	15.25	0.0084	0.886	2.646	188.07	166.647	20.5
7	17.5	0.0106	0.867	2.951	174.31	151.077	19
8	19.5	0.0114	0.845	2.791	185.32	156.603	20.2
9	21.75	0.0125	0.853	3.168	188.07	160.426	20.5
10	24.75	0.0051	0.919	1.912	493.21	453.062	21
11	27.25	0.0056	0.920	2.104	493.21	453.995	21
12	29	0.0061	0.902	2.108	493.21	444.956	21
13	32.5	0.0053	0.926	2.022	624.22	577.834	21
14	37.5	0.0065	0.916	1.652	624.22	571.682	21

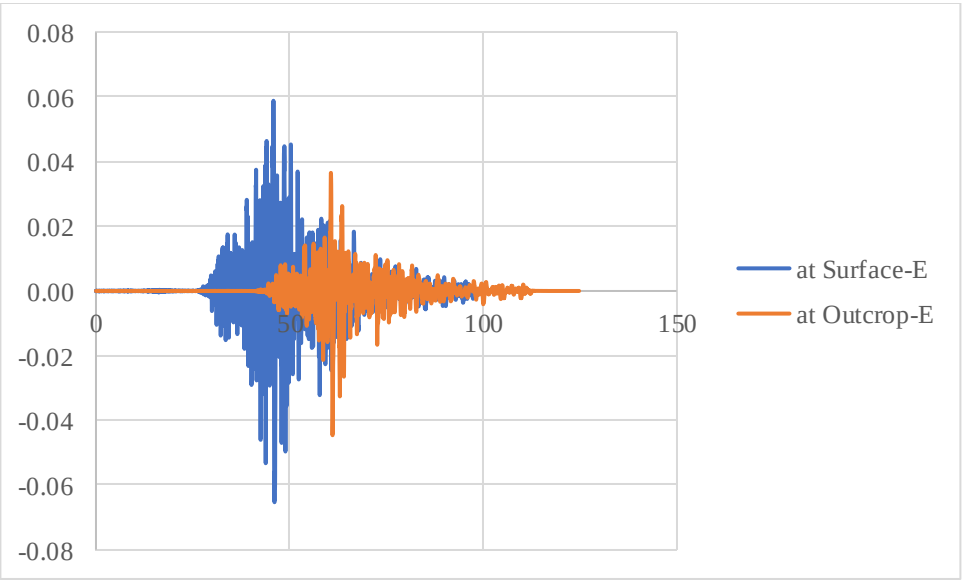


Figure 4.6 E component of the acceleration at the surface and outcrop

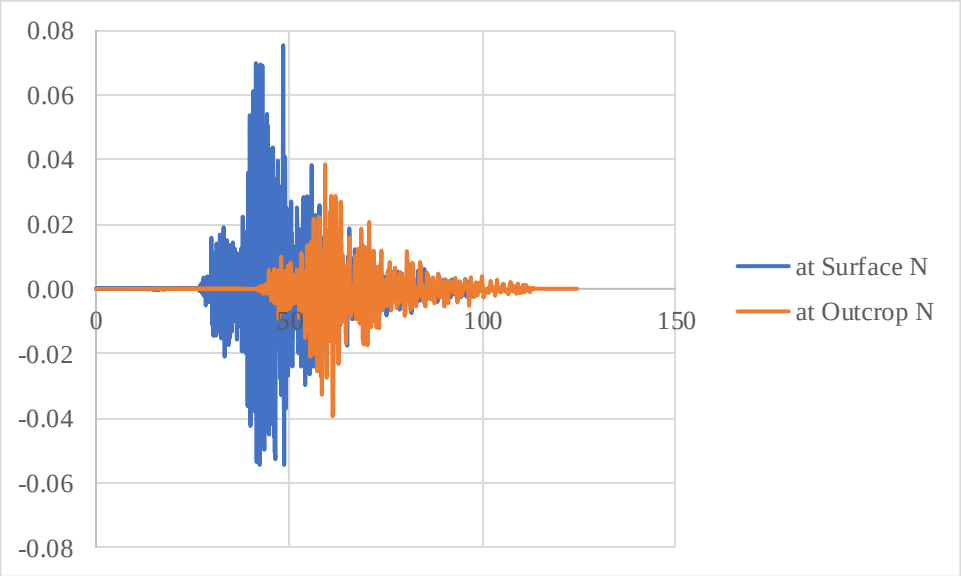


Figure 4.7 N component of the acceleration at the surface and outcrop

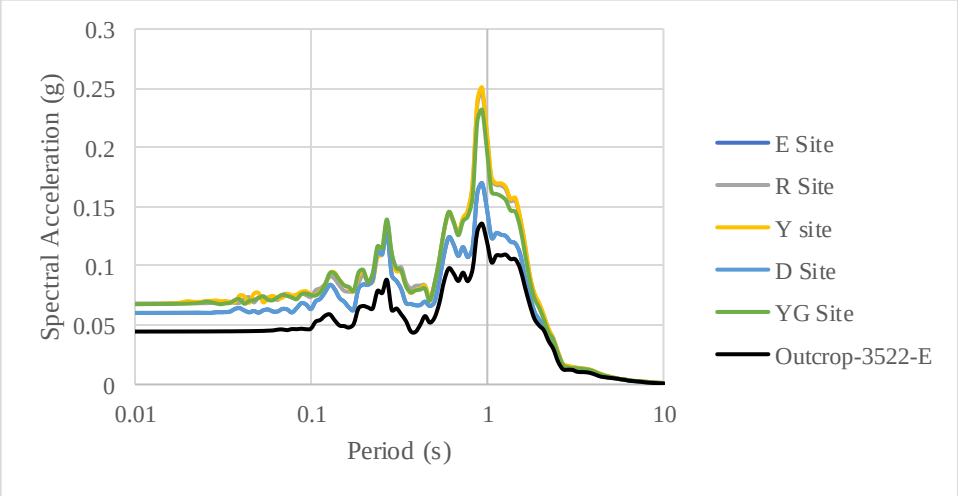


Figure 4.8 Spectral Acceleration-period for different local soil sites according to component of outcrop E

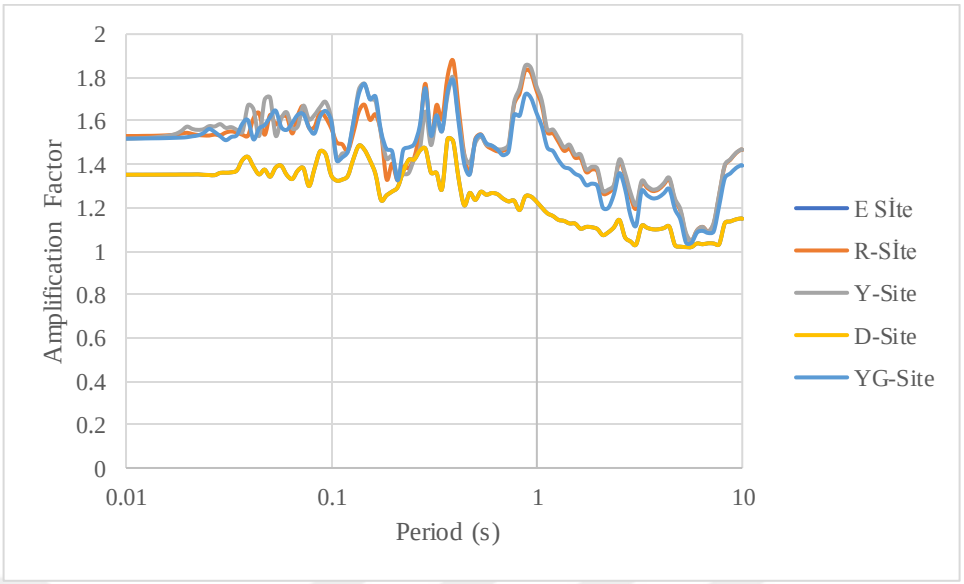


Figure 4.9 Amplification Factor for different local soil sites according to component outcrop-E

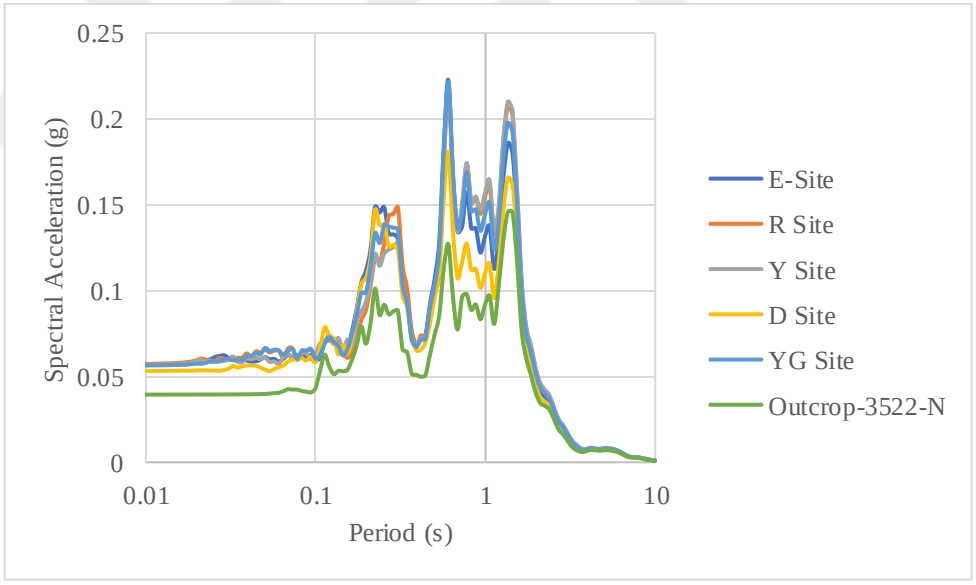


Figure 4.10 Spectral Acceleration-period for different local soil according to component of outcrop N

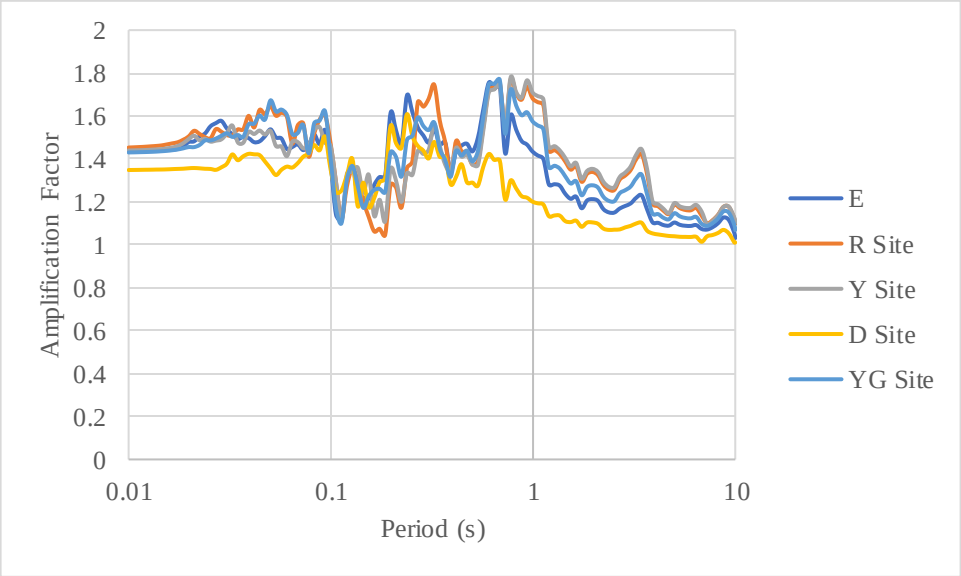


Figure 4.11 Amplification factor (AF) for different local soil sites according to component outcrop N

4.2 CASE-2 (Comparison of MKZ & GQ/H models)

It is known that model GQ/H model can predict target shear strength more accurately than MKZ model. The analysis results may not be accurate since the MKZ model overestimate or underestimate target shear strength. Models depended on MKZ and GQ/H models were created via the DEEPSOIL program at R site. R field has two impedance differences at 12 m and 38 m. Figure 4.12 shows the variation of shear wave velocity with depth. Figure 4.13 shows the variation of target shear strength with depth for two backbone models. The acceleration time record of the N component in the outcrop obtained by the deconvolution method was used for the analyses. The outcrop E component of this record shown in Figure 4.7 was used by scaling to 0.15g. The results of analyses obtained from the two models are compared and discussed.

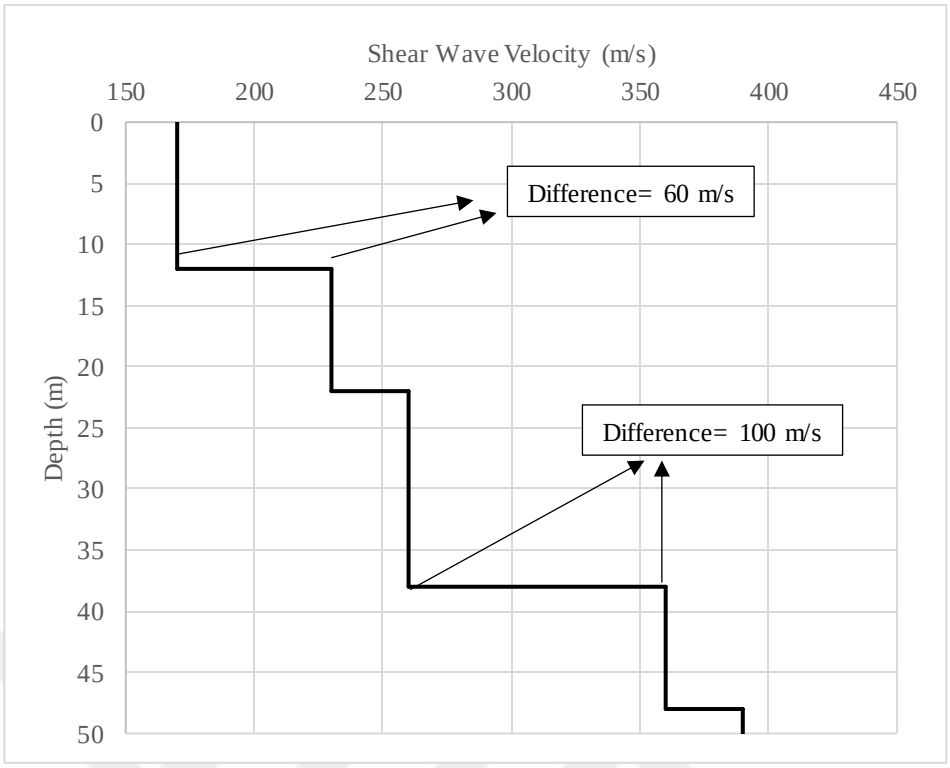


Figure 4.12 Variation of shear wave velocity with depth for R site

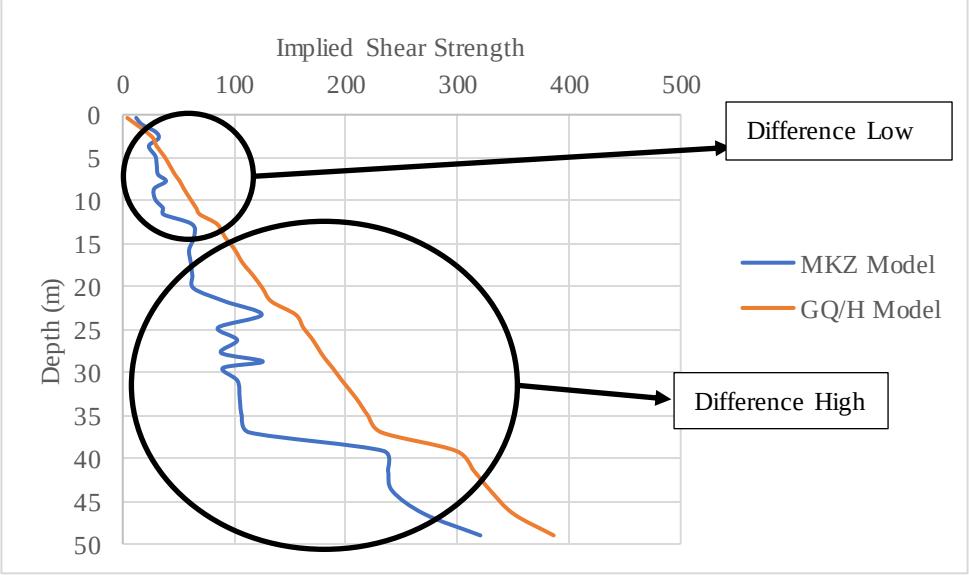


Figure 4.13 Comparison of implied shear strength for R site according to backbone models

4.2.1 Result of Analysis

As the impedance difference at 12 is more effective on the results (PGA, shear strain) than estimated shear strength difference between models, the MKZ model predicts higher shear strain, PGA values than the GQ/H model at 12 meters with an impedance difference, as illustrated in Figures 4.14, 4.15. Despite the significant differences in impedance and target shear strength at different depths in the soil profile, the MKZ and GQ/H models predict approximately the same peak ground acceleration (PGA) and shear stress values at a depth of 38 meters, as illustrated in Figures 44.14, 4.15. This may be due to the fact that, at this particular depth, the effective stress has a greater influence on the analysis results than the target shear strength and impedance difference. The MKZ model predicts approximately the same excess pore water pressure values as the GQ/H model at near surface layers, as illustrated in Figure 4.16. The MKZ model predicts higher excess pore water pressure values than the GQ/H model at layers away from surface, as illustrated in Figure 4.16, due to estimated shear strength difference between models. The Figure 4.17 shows that MKZ model predicts higher approximately same spectral acceleration values as GQ/H model.

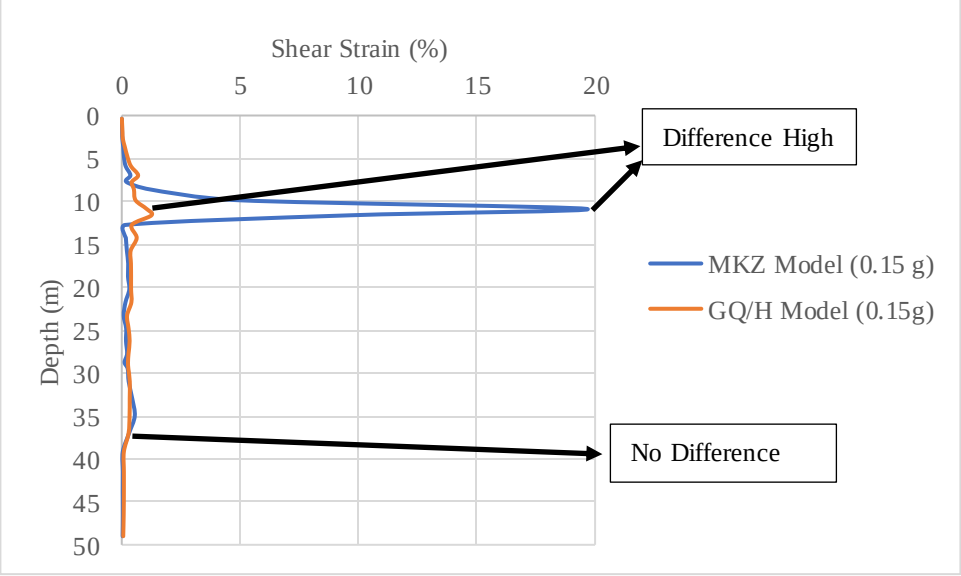


Figure 4.14 Comparison of PGA (g) for R site according to backbone models

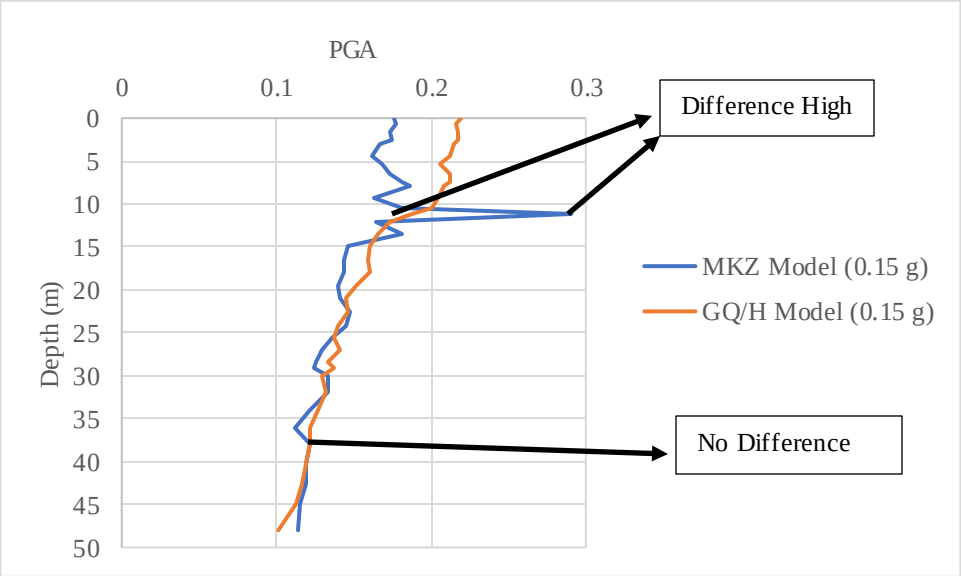


Figure 4.15 Comparison of PGA (g) for R site according to backbone models

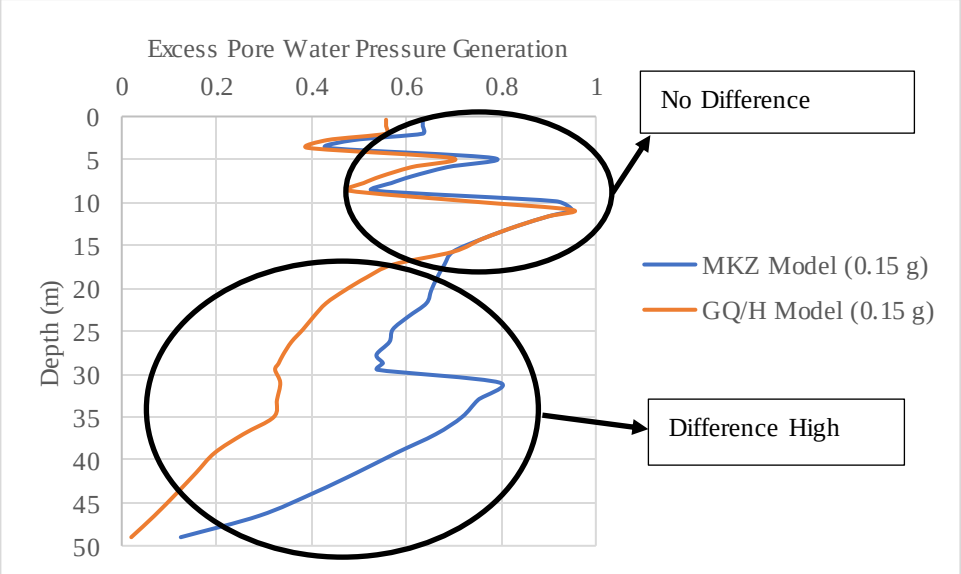


Figure 4.16 Comparison of PWP generation for R site according to backbone models

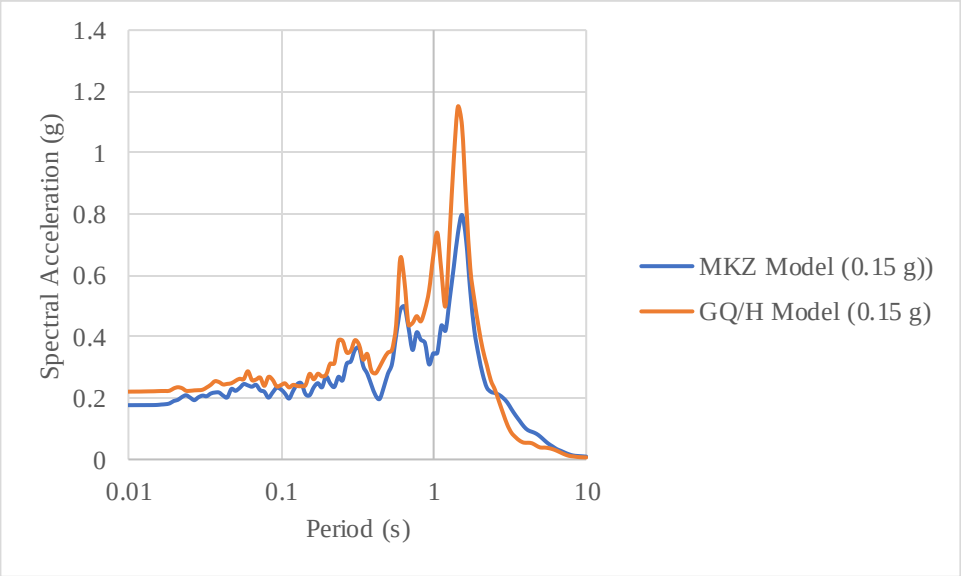


Figure 4.17 Comparison of spectral acceleration generation for R site according to backbone models

4.3 CASE-3 (Effect of soil softening and liquefaction on design response spectra)

The effect of degradation in soil strength on the variation of predominant period acceleration-time records with different predominant periods has been investigated at for E, R, and YG sites. It has been shown that liquefaction or softening of the soil changes the frequency content and causes amplification effects in the long period section. Varying excess pore water generation with depth, varying predominant period of input motions with depth, computed spectral acceleration, and varying maximum velocity/maximum acceleration have been plotted for E, YG, and R sites. The interpretation of the results obtained from the analysis has been given in the conclusion section.

4.3.1 Input Motion Selection

Records have been chosen from the NGA earthquake database (peer.berkeley.edu). The NGA-West2 database has chosen for use as base motions in SRA approximating for active crustal areas. The selection of records has been determined according to fault type, the amplitude of magnitude, shear wave velocity, and damping. Appropriate base motions were chosen from soil profile with an average shear wave velocity in the top 30 m ($V_{s,30}$) greater than 400 m/s. Fault type has been taken strike-slip and normal fay

type. Adjusting of records have been scaled according to minimize MSE. The weight function on scaling was taken from the period interval of 0.2T to 1.5 T. Fundamental period of the structure, T, is 0.7 sec. Input response spectra time for seismic SRA has been chosen to adjust a target response spectrum determined for rock site conditions. The main characteristics of input motions have been shown in Table 4.3.

Table 4.3 Properties of input motions

Event	Year	Station	Magnitude	Fault Type	Predominant Period	Scaled Arias Intensity (m/s)	Max PGA
Umbria Marche, Italy	1997	Bevagna	6	Normal	0.52	3.97	0.332
Chi-Chi, Taiwan-04	1999	CHY029	6.2	Strike Slip	0.18	1.308	0.27
Chi-Chi, Taiwan-04	1999	CHY080	6.2	Strike Slip	0.88	2.218	0.379
Düzce, Turkey	1999	Lamont 1061	7.14	Strike Slip	0.32	3.712	0.512
Manjil, Iran	1990	Abbar	7.37	Strike Slip	0.16	3.867	0.47

4.3.2 Results of Analysis

The Figures 4.18, 4.19, and 4.20 show that variation of excess pore water generation with depth. The figures 4.21, 4.22, and 4.23 show that the effect of excess pore water generation on variation of predominant period of input motions with depth. The reasons for the change in predominant periods of the input motions from the base to the surface shown in Figures 4.21, 4.22, and 4.23 are explained by the generation of excess pore water pressure, the degradation in soil strength, and the alternating profile structure formed by different soil types in the field profiles. Based on these reasons, it has been concluded that the dominant periods of the input motions increase as they propagate from the base to the surface and reach up to 2 seconds on the surface. As shown in Figures 4.21, 4.22, and 4.23, input motions at the base with low dominant periods result in greater changes in excess pore water pressure generation compared to those with high dominant periods at the base. Figures 4.24, 4.25, and 4.26 compare the

design spectrum with the spectral accelerations obtained from analysis results at different sites. Although the obtained spectral accelerations show peak values in some periods that exceed the design spectrum, they are generally below the design spectrum. Although some obtained spectral acceleration values exceed the design spectrum in the long period region, this phenomenon is explained by the softening and liquefaction of the soil. The reasons for the change in the ratio of the maximum velocity of the input motions to the maximum accelerations shown in Figures 4.27, 4.28, and 4.28 from the base to the surface are explained by the decrease in soil strength due to the generation of pore water and the alternating profile structure formed by different soil types in the field profiles, as well as the decrease in shear wave velocity from the base to the surface.

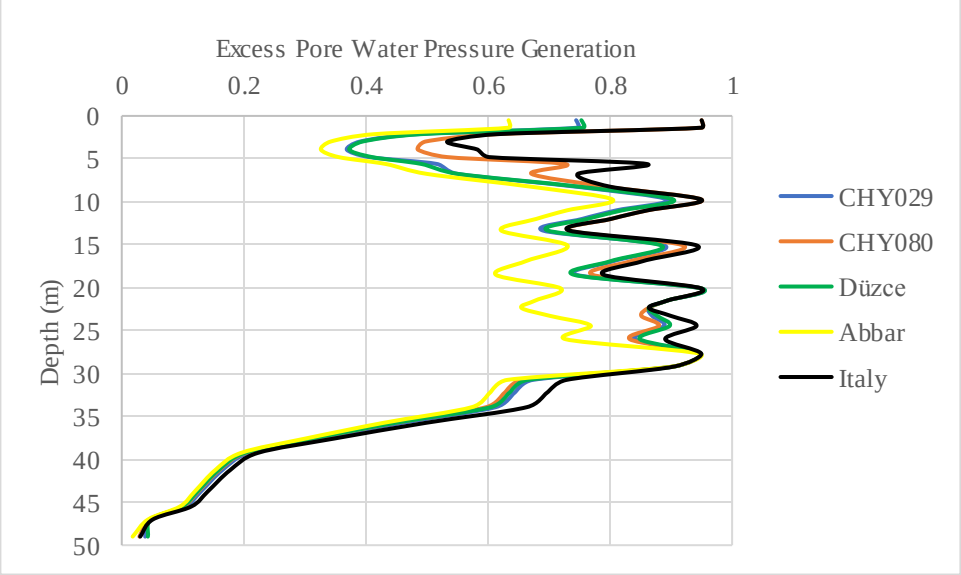


Figure 4.18 Variation excess pore water pressure generation with depth E

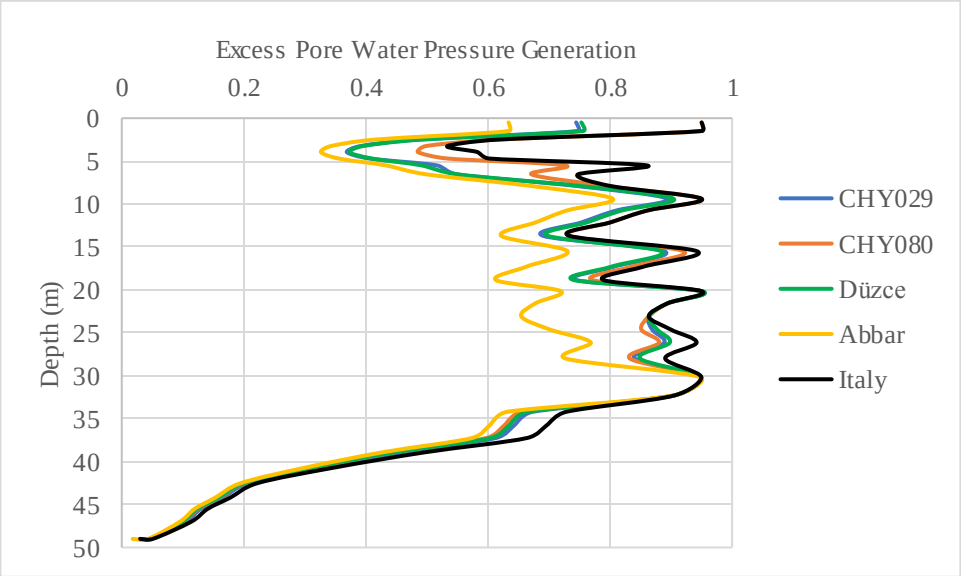


Figure 4.19 Variation excess pore water pressure generation with depth YG site

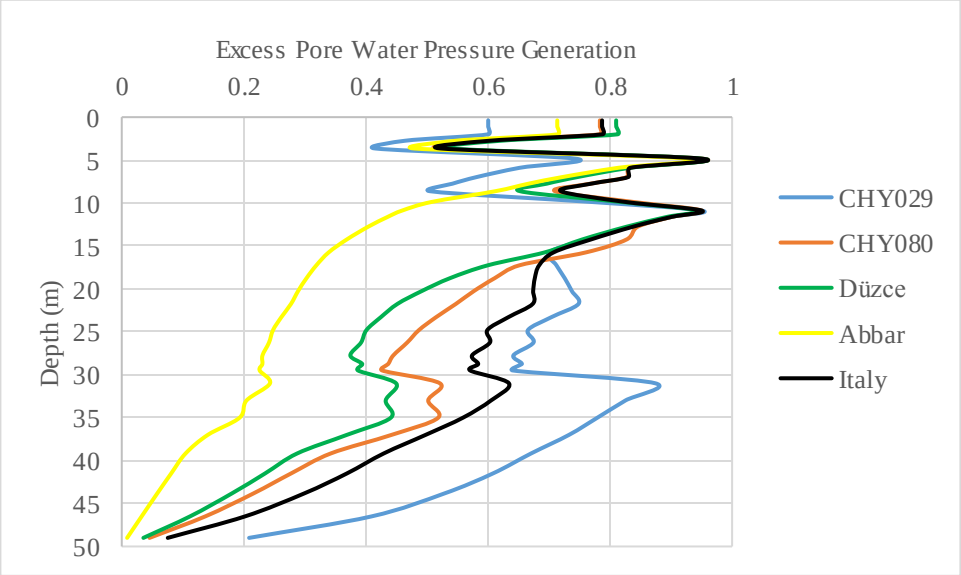


Figure 4.20 Variation excess pore water pressure generation with depth for R site

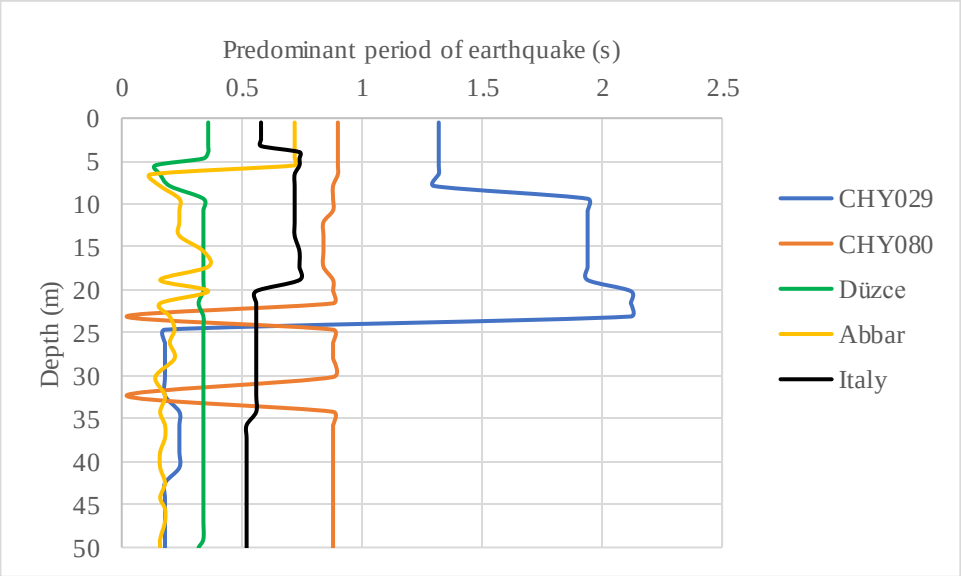


Figure 4.21 Variation of predominant period of input motions with depth E

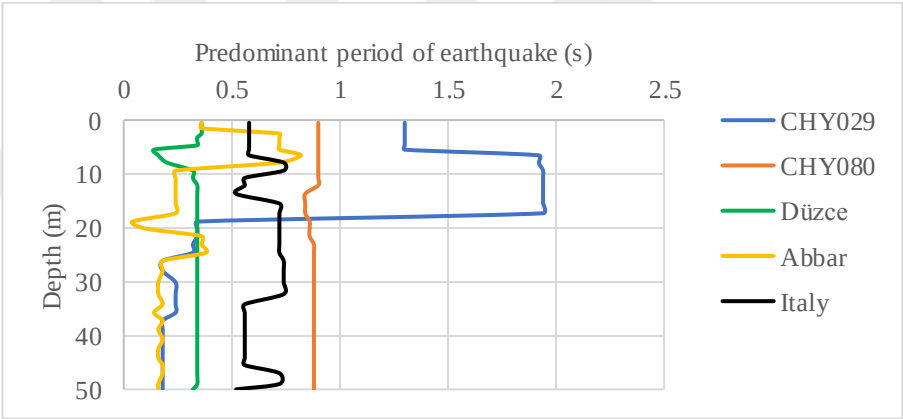


Figure 4.22 Variation of predominant period of input motions with depth for YG site

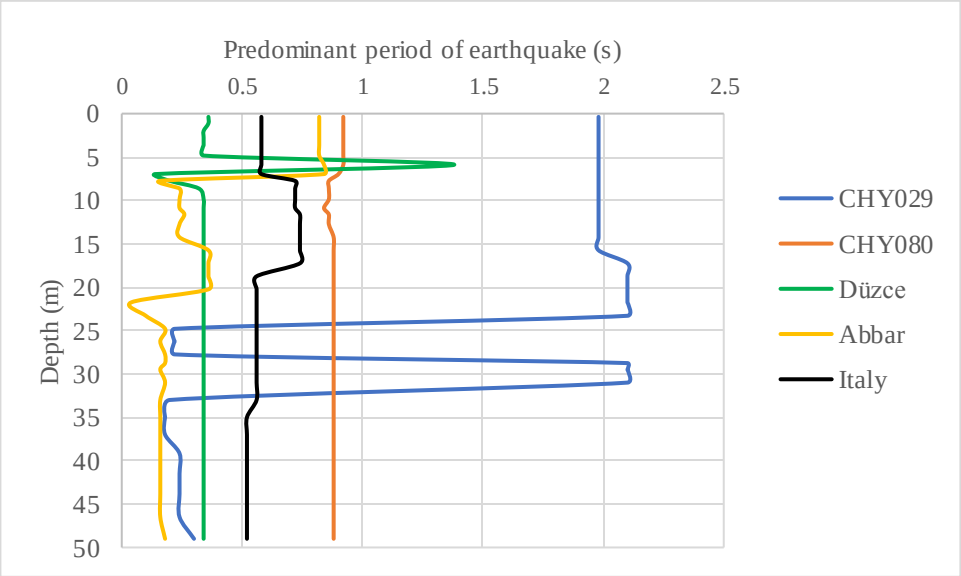


Figure 4.23 Variation of predominant period of input motions with depth for R site

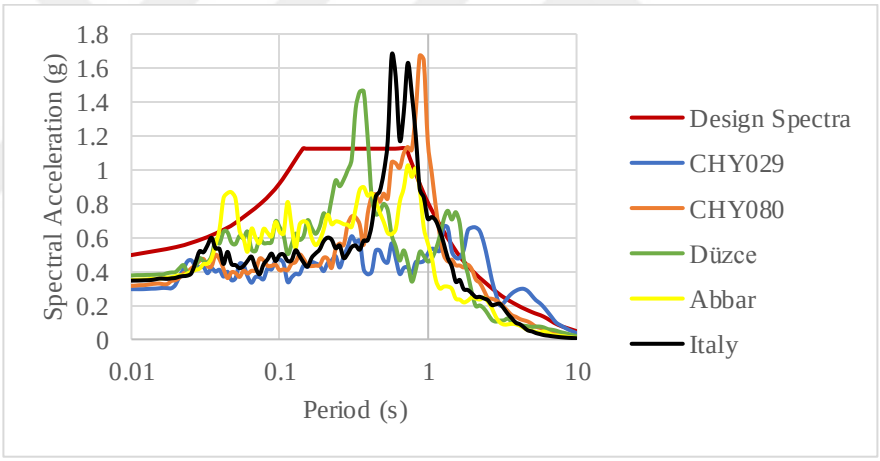


Figure 4.24 Spectral acceleration-period graph E

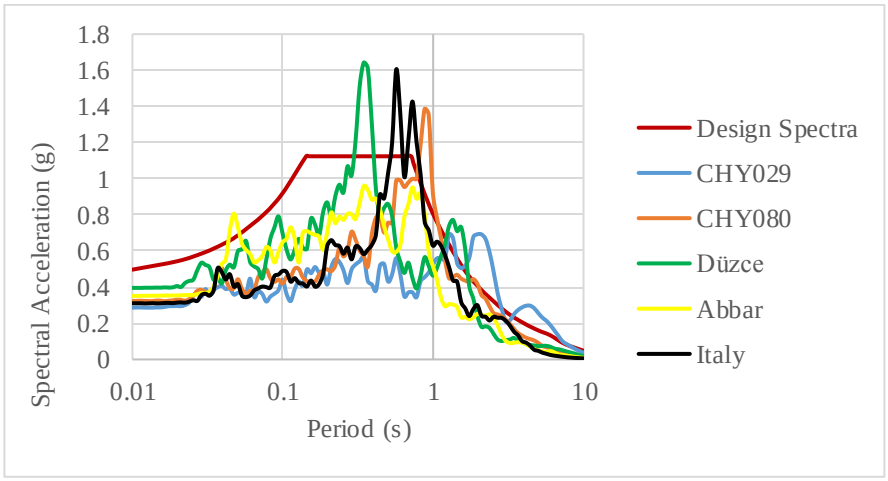


Figure 4.25 Spectral Acceleration-period graph for YG site

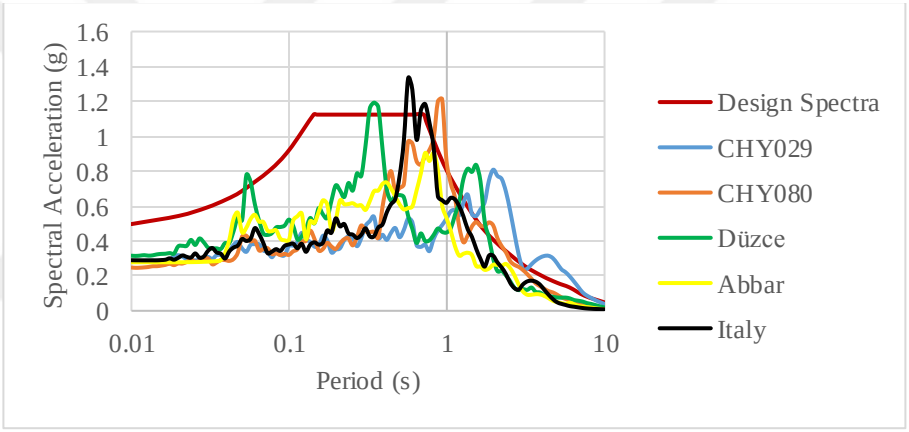


Figure 4.26 Spectral acceleration-period graph for R site

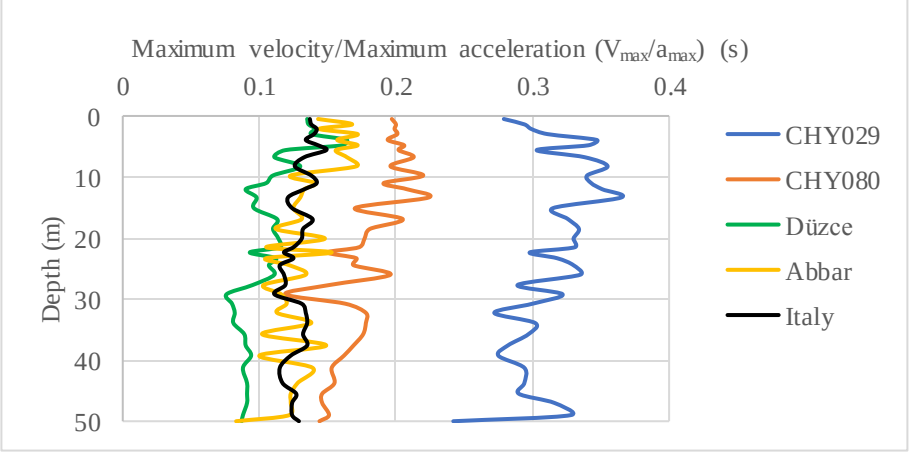


Figure 4.27 Variation of maximum velocity/maximum acceleration with depth E

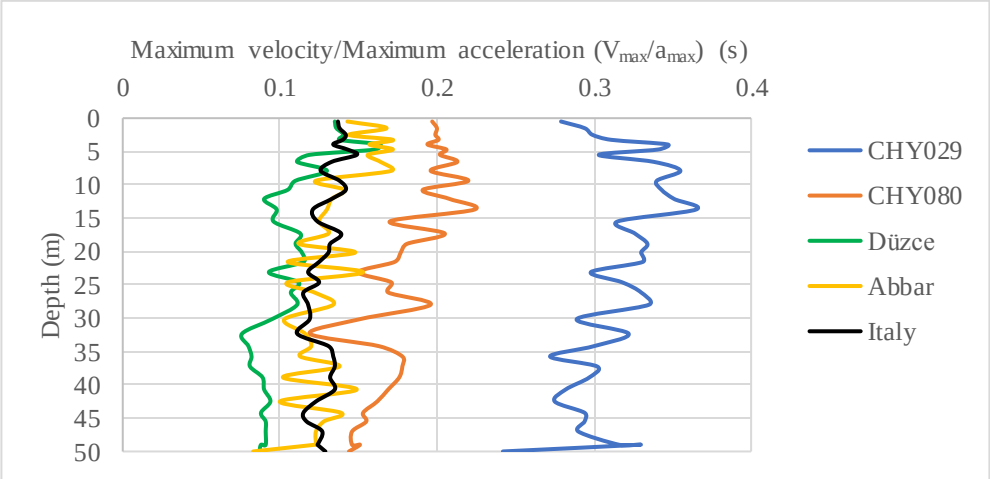


Figure 4.28 Variation of maximum velocity/maximum acceleration with depth for YG site

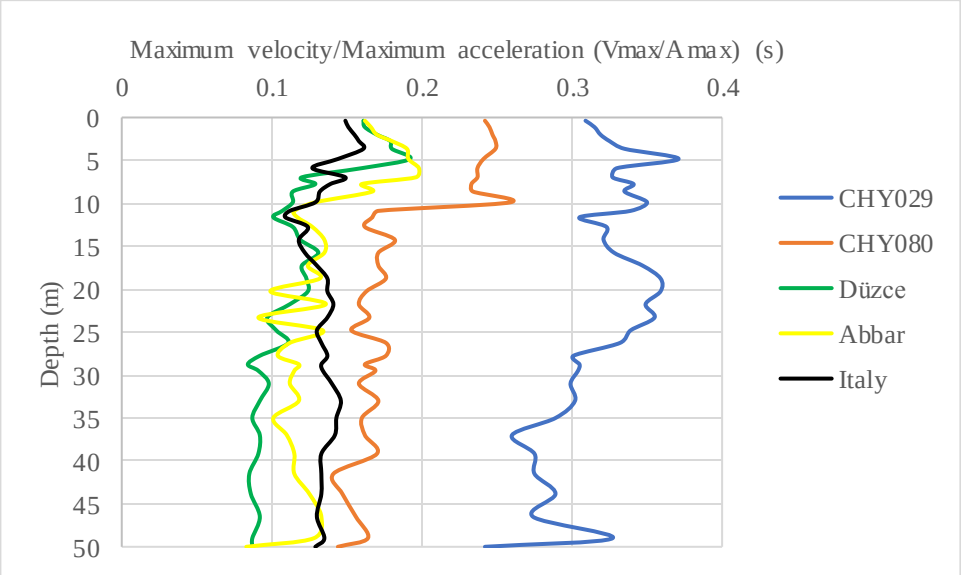


Figure 4.29 Variation of maximum velocity/maximum acceleration with depth for R site

CHAPTER 5
CONCLUSIONS AND RECOMMENDATIONS

The effects of local soil conditions on the 2020 Samos Earthquake have been shown in five site profiles consisting of alluvial soils (with alternating soil type and from low to medium plasticity clays) in the Bayraklı region. The surface acceleration-time records of the 2020 Samos Earthquake at the Çamdibi station have been converted to depth, representing the ZC soil class using deconvolution technique for the E and N components. The obtained acceleration-time records have been used to investigate the spectral accelerations and amplification factors on the surface in five sites. The results of analyses have shown that earthquake motion with low arias intensity and low peak ground acceleration at the base resulted in higher arias intensity and peak ground acceleration on the surface. The shear modulus of clayey soil profiles with plasticity decreases during earthquake. However, the damping of the soil does not try to absorb the earthquake's energy. In other words, the damping of the soil is not activated because the ground motion's energy is low. Weak ground motions, such as the 2020 Samos Earthquake, cause amplification of spectral acceleration values. While designing the structures, it is mandatory to play important role to the design of the structures in the period range that may be subject to dynamic resonance.

When site specific dynamic soil behavior analyses have been conducted in DEEPSOIL software, the significant of selecting an appropriate backbone model that defines the nonlinear stress-strain relationships of the soil has been shown. The MKZ model and GQ/H models have been used for analyses, and results of analyses estimated by the models have been compared. For the analyses, the R site with significantly variation shear wave velocity at 12 and 38 m has been selected. There is no significant difference between the shear strengths estimated by the MKZ and GQ/H models at shallow depths (first 15 m), and there is a significant difference in shear wave velocity between the layers. The effective stresses of both the MKZ and GQ/H models increase from the surface to the base of the entire site profile. The MKZ model estimates higher peak ground acceleration and shear strain values in the layers near the surface than GQ/H model. The results of analyses show that the difference in shear wave velocity

between the layers at 12 m has greater effect on peak ground acceleration and shear strain values than shear strength and effective stress for the MKZ model. The MKZ model estimates approximately the same excess pore water pressure generation values as the GQ/H model at shallow depths (first 15 m). The results of analyses show that the shear strength is more effective on the excess pore water pressure generation than the difference in shear wave velocity and effective stress at shallow depths (first 15 m) for MKZ model.

There is a significant difference between the shear strengths estimated by the MKZ and GQ/H models at depths far from the surface (between 15 m and 50 m), and there is a significant difference in the shear wave velocities between layers (at 38 m). The effective stress is the same for both the MKZ and GQ/H models increase from the surface to the base of entire site profile. The MKZ model predicts approximately the same peak ground acceleration and shear strain values as the GQ/H model in the deeper layers. The results of analyses show that the effect of effective stress at deeper layers are greater than that of the shear strength difference at models and the shear wave velocity between the layers at the depth of 38 m on shear strain and peak ground acceleration for the MKZ model. The MKZ model estimates higher excess pore water generation values at deeper layers than GQ/H model. The results of analyses have shown that the effect of shear strength difference estimated by models on excess pore water pressure generation are greater than that of the shear wave velocity difference between deeper layers and effective stress for the MKZ model.

The MKZ model has predicted to result in higher shear strain and peak ground acceleration results than GQ/H model, which in turn has predicted to result in higher spectral acceleration values in the GQ/H model compared to the MKZ model at surface. It has demonstrated that there is an inverse relationship between the predictions of the MKZ model and GQ/H models with respect to shear strain, PGA, and excess pore water pressure values on the hand, and spectral acceleration values on the other hand. Generally, as shear strain and peak ground acceleration values increase, the ability to absorb earthquake motion may also increase.

The MKZ model can produce unrealistic results when performing site-specific dynamic soil behavior analyses due to its incorrect estimated target shear strength. Deformation, shear strain, spectral acceleration, excess pore water generation, and peak ground acceleration results can be overestimated or underestimated, resulting in incorrect design. It shows that accurate estimation of soil stiffness is crucial in site-specific soil behavior analysis.

Predominant period of input motions varies with depth, from the base to surface. The reasons for the change in predominant periods of the input motions from the base to the surface are explained by the generation of excess pore water pressure, the decrease in soil strength, and the alternating profile structure formed by different soil types in the field profiles. There is an interaction between reduction of soil strength and the dominant period of input motion Based on these reasons, it has been concluded that the dominant periods of the input movements increase as they propagate from the base to the surface and reach up to 2 seconds on the surface. Input motions at the base with low predominant periods result in greater changes, specifically excess pore water pressure generation, after reaching the surface compared to those with high predominant periods at the base. Input motions with a low predominant period can affect the properties of input motions and amplify the properties of input motions and soil response more than input motions with a high predominant period during a seismic event The spectral accelerations obtained from analysis results at different sites compare with the design spectrum. Although the obtained spectral accelerations show peak values in some periods that exceed the design spectrum, they are generally below the design spectrum. Although some obtained spectral acceleration values exceed the design spectrum in the long period region, this phenomenon is explained by the softening and liquefaction of the soil. The reasons for the change in the ratio of the maximum velocity of the input motions to the maximum accelerations shown from the base to the surface are explained by the decrease in soil strength due to the generation of pore water and the alternating profile structure formed by different soil types in the field profiles, as well as the decrease in shear wave velocity from the base to the surface. Soil profiles are often composed of alternating layers of different types of soil. For amplification and changing of the predominant period of input motions, the excess

PWP generated in sand layers may affect increase in excess pore water pressure of clay layers. It can lead to both amplification of input motion and changing the frequency of soil layers (Matasovic,1993). The change in the maximum velocity and maximum acceleration of the earthquake wave passing from a rigid layer to softer layer. The principle of conservation of energy explains this. There is an interaction between reduction of soil strength and the dominant period of input motion. The increase in the excess pore water pressure (PWP) can indeed affect the predominant period of input waves.

This thesis demonstrates the importance of accurately estimating shear strength on excess pore water pressure generation results using different backbone models. The importance of shear wave velocity, shear strength, and effective stress on peak ground acceleration, shear strain, and excess pore water pressure generation results are shown for deeper and shallow depths. Another effect on excess pore water pressure is to use the correct excess pore water model and select the parameters in these models entered the DEEPSOIL software as correct values. An energy-based excess pore water pressure model can be used for sands. The advantage of the energy-based excess pore water pressure model over the strain-based model used for sandy soil is that it has fewer parameters, and these parameters depend on the effects of shear wave velocity and fines content. Using two models, statistical studies can be conducted, and the effects of the parameters in these two models on excess pore water pressure generation results can be compared for sandy soils. Additionally, the effects of alternating soil types (Clay-Sand) in the layered soil profile on each other (such as changing the frequency content of earthquake motion) can be examined during excess pore water pressure generation.

REFERENCES

Altunevlek, D. Sensitivity of dynamic site response to excess pore pressure generation parameters. M.Sc. Thesis. Dokuz Eylül University.

Borcherdt, R. D. (1994b). Estimates of site dependent response spectra for design (methodology and justification). Earthquake Spectra, 10, 617-653.

Carlton, B. (2014). An improved description of the seismic response of sites with high plasticity soils, organic clays, and deep soft soil deposits. PhD Thesis. University of California, Berkeley.

Darendeli, M. B. (2001). Development of a new family of normalized modulus reduction and material damping curves. PhD Thesis, University of Texas at Austin.

Dobry, R. (1982). Prediction of pore water pressure buildup and liquefaction of sands during earthqukes by the cyclic strain method[M]. US Department of Commerce, National Bureau of Standards.

Gang, L. (2013). Study of the grain size distribution on the mechanical behavior of granular materials. PhD Dissertation, University de Nantes.

Groholski, D. R., Y.M.A, Hashash, Kim, B., Musgrove, M., Harmon, J., Stewart, J.P. (2016). A Simplified non-linear shear model to represent small-strain nonlinearity and soil strength in 1-D seismic site response analysis. Journal Geotechnical Geoenvironmental Engineering,10.1061/(ASCE)GT.1943-5606.0001496, 04016042.

Hardin, B. O., and Drnevich, V. P. (1972). Shear modulus and damping in soils: Design equations and curves. Journal of the Soil Mechanics and Foundation Division, ASCE, Vol. 98, No. SM7, 667-692.

Hardin, B. O., and Drnevich, V. P. (1972). Shear modulus and damping in soils: Measurement and parameter effects. Journal Soil Mechanics Foundation Division., ASCE, 98(6).

Hashash, Y. M. A., & D. Park (2001). Non-linear one-dimensional seismic ground motion propagation in the Mississippi embayment. Engineering Geology, 62(1-3), 185-206.

Hashash, Y.M.A., Musgrove, M.I., Harmon, J.A., Ilhan, O., Xing, G., Numanoglu, O., Groholski, D.R., Phillips, C.A., & Park, D. (2020). DEEPSOIL 7.0, User Manual. Urbana, IL, Board of Trustees of University of Illinois at Urbana-Champaign

Hazirbaba, K. (2005). Pore pressure generation characteristics of sands and silty sands: A strain approach. PhD Dissertation, University of Texas at Austin

Idriss, I. M. (1990). Response of soft soil sites during earthquakes. Provision Symposium to Honor Professor H. B. Seed, Berkeley, California.

Isenhower, W. M. (1979). Torsional simple shear resonant column properties of San Francisco Bay mud. Thesis presented to the faculty of the graduate school of the University of Texas at Austin in partial fulfillment of the requirements of the degree of Master of Science in engineering, December.

Ishibashi, I., & X. Zhang (1993). Unified dynamic shear moduli and damping ratios of sand and clay. Soils and Foundations 33(1), 182-191.

Ishihara, K. (1996). Soil behavior in earthquake geotechnics. Clarendon, Oxford, U.

Kokusho, T., Yoshida, Y., and Esashi, T. (1982). Dynamic properties of soft clay for wide strain range. Soils Foundation., 22(4), 1-18.

Kondner, R. L., and Zelasko, J. S. (1963). Hyperbolic stress-strain formulation of sands. Second pan American Conference on Soil Mechanism and Foundation Engineering, Sao Paulo, Brazil, 289-324.

Kramer, S. L. (1996). Geotechnical earthquake engineering. Prentice-Hall, Inc., Upper Saddle River, N. J.

Park, D.and Y. M. A. Hashash (2004). Soil damping formulation in nonlinear time domain site response analysis. Journal of Earthquake Engineering, 8(2), 249-274.

PEER (2010). PEER strong motion database, California, Berkeley, USA. https://peer.berkeley.edu.

Phillips, C., and Y. M. A. Hashash. (2009). Damping formulation for non-linear 1D site response analyses. Soil Dynamics and Earthquake Engineering, 29(7), 1143-1158.

Pyke, R. (1979). Nonlinear soil models for irregular cyclic loadings. Journal of the Geotechnical Engineering Division, 105(11).

Masing. G. (1926). Eignespannungen and verfestigung beim messing. Proceedings, 2nd Intoduction Congress on Applied Mechanics, Zurich, Switzerland.

Matasovic, N. (1993). Seismic response of composite horizontally layered soil deposits. Ph.D. Thesis, University of California, Los Angeles.

Matasovic, N., and M., Vucetic (1993). Cyclic characterization of liquefiable sands. ASCE Journal of Geotechnical and Geoenvironmental Engineering, Vol. 119, No. 11, pp 1805-1822.

Matasovic, N., and M, Vucetic (1995). Generalized cyclic degradation pore pressure generation model for clays. ASCE Journal of Geotechnical and Geoenvironmental Engineering, Vol. 121, No. 1, pp33-42.

Mei, X., Olson, S. M., and Hashash, Y. M. A. (2015). Empirical curve fitting parameters for a porewater pressure generation model for use in 1-D effective stress-based site response analysis. 6 th International Conference on Earthquake Geotechnical Engineering, 1-4 November 2015, Christchurch, New Zealand.

Newmark, N. M. (1959). A method of computation for structural dynamics. Journal Engineering Mechanical Division, ASCE, 67-94.

Ramberg, W., and Osgood, W.R. (1943). Description of stress-strain curves by threes parameters. Technical Note 902, National Advisory Committee for Aeronautics, Washington, D.

Rayleigh, J. W. S and R. B. Lindsay. (1945). The theory of sound, Dover Publications, New York.

Schnabel, P. B., Lysmer, J., and Seed, H. B. (1972). SHAKE: A computer program for earthquake analysis of horizontally layered sites. Report No. EERC 72-12, College of Engineering, University of California, Berkeley, USA.

Seed, H. B and Alonso, J. L (1974). Soil-structure interaction effects in the Caracas earthquake of 1967. Report No. 73023, Earthquake Engineering Research Center, Engineering Department, University of California, Berkeley, CA.

Seed, H. B., Murarka, R., Lysmer, J., and Idriss, I. M. (1976a). Relationships between maximum acceleration, maximum velocity, distance from source and local site conditions for moderately strong earthquakes. Bull. Seism. Soc. Am., 66, 1323-1342.

Seed, H. B., Ugas, C., and Lysmer, J. (1976b). Site dependent spectra for earthquake-resistant design. Bull. Seism. Soc. Am., 66, 221-244.

Seed, H. B., Wong., R. T., and Idriss., I. M., and Tokimatsu., K. (1984). Moduli and damping factors analyse of cohesionless soils. Report UCB/EERC-84/14, Earthquake Engineering Research Center, University of California, Berkeley, CA.

Seed, H. B., Wong, R.T., Idriss, I.M., & Tokimatsu, K. (1986). Moduli and damping factors for dynamic analyses of cohesionless soils. Journal of Geotechnical Engineering 112(11), 1016-1032.

Seed, H. B., Romo., M. P., Sun., J., Jaıme., A., Lysmer., J. (1987). Relationships between soil conditions and earthquake ground motions in Mexico City in the earthquake of September 19, 1985. Report UCB/EERC-87/15, Earthquake Engineering Research Center, University of California, Berkeley, CA.

Silva, W. (1988). Soil response to earthquake ground motion: Final report. EPRI-NP-5747 ON: TI88920246.

Stokoe, K. H. and Lodde, P. F. (1978). Dynamic response of San Francisco Bay mud. Proceedings, ASCE Special Conference on Earthquake Engineering and Soil Dynamics, Pasadena, California, Volume 2, June, pp. 940-959.

Tan, K. Y., and Vucetic, M. (1989). Behavior of medium and low plasticity clays under cyclic simple shear conditions. Provision Fourth Introduction Conference on

Soil Dynamics and Earthquake Engineering, Soil dynamics and liquefaction, 131-141.

Terzaghi, K. (1925). Erdbaumechanik auf bodenphysikalischher grundlage. Franz, Deutice, Leipzig and Wien.

TBDY (2018). Turkey Building Earthquake Code.

Vucetic, M. (1988). Normalized behavior of offshore clay under uniform cyclic loading. Canadian Geotechnical Journal, 25, 33-41.

Vucetic, M. (1994). Cyclic characterization for seismic regions based on plasticity index. Provision XIII International (World) Conference on Soil Mechanics and Foundation Engineering, New Delhi, India, Vol 1, 329-332.

Vucetic, M., and Dobry, R. (1986). Pore pressure buildup and liquefaction of level sandy sites during earthquakes. Research Report, Rensselaer Polytechnic Institute, Troy, New York, 616 p.

Vucetic, M., and Dobry, R. (1988). Degradation of marine clays under cyclic loading. Journal Geotechnical Engineering, ASCE, 114(2), 133-149.

Vucetic, M. and Dobry, R. (1991). Effect of soil plasticity on cyclic response. Journal of Geotechnical Engineering, 117(1), 87-107.

Zen, K., Umehara, Y., and Hamada, K. (1978). Laboratory tests and in-situ seismic survey on vibratory shear modulus of clayey soils with various plasticity. Proceedings, Fifth Japan Earthquake Engineering Symposium, Tokyo, Japan, November, pp. 721-728.